NASA ONLY

STUDIES OF INTERFACE DAMPING

SUMMARY TECHNICAL REPORT NO. 1

(25 May 1967 - 24 August 1967)

Contract No: NAS5-10310
SwRI Project No. 02-2033

by

U. S. Lindholm
R. D. Brown
L. M. Yeakley

Prepared for

Goddard Space Flight Center
Greenbelt, Maryland

July 1968

SOUTHWEST RESEARCH INSTITUTE
SAN ANTONIO HOUSTON

SOUTHWEST RESEARCH INSTITUTE
8500 Culebra Road, San Antonio, Texas 78228

STUDIES OF INTERFACE DAMPING

SUMMARY TECHNICAL REPORT NO. 1
(25 May 1967 - 24 August 1967)

Contract No: NAS5-10310
SwRI Project No. 02-2033

by

U. S. Lindholm
R. D. Brown
L. M. Yeakley

Prepared for

Goddard Space Flight Center
Greenbelt, Maryland

July 1968

Approved:

H. Norman Abramson, Director
Department of Mechanical Sciences

ABSTRACT

For structures intended for operation in space, total structural damping may be adversely affected by the vacuum conditions. Since energy dissipation due to slip at structural interfaces is expected to be a major contributor to the overall damping, experiments have been performed in air and vacuum on small, nominally flat aluminum specimens in oscillatory sliding contact. Energy dissipation per cycle was measured for both small (microslip) and relatively large (gross slip) tangential displacements. The significant differences which could be found between tests in air and in vacuum are discussed in terms of the retention or loss of the surface oxide layer in aluminum, and the mechanical affects caused by its breakup within the interface. The results with small specimens suggest that interface damping in structures can be significantly reduced in a vacuum or in the absence of oxygen. Further studies with simple structures are recommended.

TABLE OF CONTENTS

LIST OF FIGURES

Figure No.

INTRODUCTION

As a natural consequence of the expanding space flight programs in both orbital and interplanetary flight, there arises a pressing need for design techniques, methods of analysis and data applicable to the new problems which arise in the strange environment of space. The dynamic characteristics of spacecraft structures have been receiving increasing attention of late; however, knowledge of natural frequencies and mode shapes alone is insufficient. Information on the energy dissipation characteristics of the system must be available in order to determine the ability of a structure to withstand the expected excitation.

The three basic mechanisms of energy dissipation in mechanical systems or structures are (1) internal hysteresis or material damping, (2) acoustic or radiation losses and (3) joint interface or structural assembly damping. Let us consider now the effects of the space environment, particularly that of the hard vacuum, on these energy dissipation mechanisms. Material hysteretic damping in structural metals is generally small, becoming appreciable only in highly stressed regions. Thus, that portion of the overall structural damping contributed by material losses is generally small, even in a one-atmosphere environment. To the writer's knowledge, the effect of a hard vacuum on the hysteresis losses in metals has not been studied. Vacuum effects on the fatigue life of metals have been quite extensively studied[1], however, and the results show a marked extension of fatigue life in hard vacuum. Since, for a given metal, fatigue life is generally

related to hysteresis loss per cycle, the increased fatigue life in vacuum would suggest that the energy dissipation in the metal is possibly decreased also. In the category of material damping we may also include viscoelastic coatings; materials of high internal energy loss under cyclic loading. Weight penalties generally preclude extensive use of such coatings in space applications. Also, since these materials are usually polymers, they may not be compatible with the space environment because of outgassing.

Under atmospheric conditions, acoustic or radiation damping is a major source of energy dissipation, particularly in thin-walled or lightweight structures. This loss mechanism will be completely removed in the absence of a surrounding atmosphere.

This leaves interface or joint damping as probably the major contributor to energy dissipation or structural damping in space. However, the hard vacuum may have considerable influence on this mechanism also. For instance, one recently proposed mechanism of energy dissipation in vibrating joints at high frequencies, that of gas pumping in the joints[2], will be absent. The dominant remaining mechanism is the loss produced by tangential slip at the interface of the joint. It is generally assumed that this tangential slip is governed by the action of Coulomb type friction. It is this last mechanism of interface slip damping in joints that is the object of the present study.

Since interface slip damping would appear, then, to be of considerable importance for structures intended to operate in space environments, our objective in the present study is to gain a better understanding of the

mechanisms involved so that we may be able to estimate more accurately the damping capacity of a given structure and be able to predict how damping will be affected by prolonged space exposure. Such understanding may lead to methods of maintaining adequate energy dissipation in space for a given configuration, without sacrificing other structural considerations.

PRELIMINARY DISCUSSION

Two surfaces, pressed together under normal pressure and subject to forces tangential to the interface, will slip, i.e., undergo relative displacement, if the local shear stress at the interface exceeds the limiting frictional forces. For Coulomb friction, the limiting shear stress is given by the coefficient of friction, μ, multiplied by the pressure, p, normal to the surface. Often, the two surfaces in contact are constrained at various points or the distribution of normal or shearing stress is non-uniform. Then, the limiting shear stress may be exceeded only in limited regions of the interface. If the applied loading varies with time, these local areas of slip will grow or contract according to the stress distribution. The slip is an irreversible process, so that work must be done in order to move the slip boundary. If the load is oscillatory, the slip region will grow and contract each cycle and a certain amount of energy will be dissipated. If the limiting shear stress is exceeded everywhere at the interface, gross motion or sliding will occur between the two bodies in contact if they are not constrained.

For certain simple configurations, elastic* analyses are available which yield the load-displacement relationships from which the hysteresis loop and energy dissipation per cycle can be calculated. It is useful to review a few of these to see the relationship between the various parameters.

First, let us look at two simple cantilever beam configurations which appear similar but whose behavior is quite different. Take the simple built-up cantilever beam of Pian and Hallowell[3] shown in Figure 1a and the two component cantilever beam of Goodman and Klumpp[4] shown in Figure 1b. The shapes of the theoretical hysteresis loops under completely reversed cyclic loading are given below each beam. In both cases the normal pressure, p, is assumed uniform over the interface. Without going through the details of the derivation, let us examine the form of the equations for energy dissipation per cycle, ΔE, for completely reversed oscillatory loading. For the beam of Figure 1a,

$$\Delta E = \left(\frac{4}{3}\right)\frac{F_m{}^3 \ell^3}{EIq}\left[1 + \frac{1}{6}\frac{h}{a} + \frac{F_m}{q}\right]^{-2} \qquad (1)$$

and for the beam of Figure 1b,

$$\Delta E = \left(\frac{2}{3}\right)\frac{q\ell^3}{EI}\left[F_m - \frac{4}{3}q\right] \; ; \quad F_m > F_s = \frac{4}{3}q \qquad (2)$$

where in each case

μ = coefficient of Coulomb friction

p = normal pressure

* While elastic analysis is used, slip is allowed to occur at the interface and thus, the results are nonlinear and hysteretic. This is analogous to elastic analysis of dislocation in metal physics.

$I = \frac{bh^3}{12}$

E = elastic modulus

F_m = maximum applied oscillatory load

a, b, h, ℓ = linear dimensions indicated in Figures 1a, b

$q = \mu p b h$

The product (μp) is the limiting shear stress at the interface according to Coulomb friction theory.

Some important differences can now be noted. For the beam of Pian and Hallowell, slip is initiated instantly for very small loads F. This slip starts at the left hand boundary of the spar cap where the shear stresses are large because of the discontinuity in section. As the applied load is increased, the boundary of the slip region moves progressively toward the free end of the beam. The shape of the hysteresis loop reflects this displacement of the slip boundary with increasing load. Equation (1) is valid only so long as the slip boundary has not displaced a distance greater than ℓ. The dissipation, in this case, is dominantly proportional to the third power of the applied load and inversely proportional to the coefficient of friction (or the normal clamping pressure). This type of dependence is characteristic of many types of joints where the instantaneous area of slip is proportional to the applied load. Summaries of many of these types are given by Goodman[5] and Kalinen, et al[6].

In contract to this, the beam configuration of Goodman and Klumpp exhibits elastic, non-dissipative behavior up to a limiting load $F_s = \frac{4}{3} q$. At this load, the limiting shear stress is reached uniformly over the length

of the beam and slip occurs. Thus, there is no gradual growth of the slip region. This results in a dissipation which is directly proportional to the first power of the applied force and also directly proportional to the coefficient of friction (or normal clamping pressure). It is important to note that for this case there is also an optimum clamping pressure, $p_o = \frac{3}{8} \frac{F_m}{\mu bh}$. This pressure maximizes the energy dissipation.

From these two examples, it can be seen that the dependence of the energy dissipation on the applied loading and the interface parameters controlling friction is influenced by the geometry of the structure. Further, in the case of nonuniform normal pressure over the joint area, as in riveted or bolted beams, Unger[7] finds that the dissipation may vary as a power of the load range, anywhere between the second and third power depending on the normal pressure distribution. Thus, for a complex structure under generalized loading, considerable difficulty can be encountered in predicting the functional relationship between interface damping and the applied loading.

Similarly, the dependence of the dissipation on the coefficient of friction is different in the two cases just cited. In a hard vacuum it is expected that the coefficient of friction will increase. For the class of problems similar to Figure 1a we could expect a decrease in the magnitude of the interface slip damping in space for equivalent excitation. However, the beam of Figure 1b would exhibit increased damping in vacuum for applied loading greater than F_s. The latter appears to be shown by the experiments of McWithey and Hayduk[8] who measured the free decay of a cantilever beam of the configuration in Figure 1b at various vacuum levels. At low tip

amplitudes the logarithmic decrement approximately doubled between one atmosphere and 9.5×10^{-8} torr.

In addition to beams, other shapes of contact surfaces have been studied. One of the earliest theoretical studies of tangential displacements prior to gross rigid body sliding was by Mindlin[9]. He considered the effect of tangential forces on elastic bodies in contact. For the case where the contacting area is a circle, for instance a sphere on a flat, Mindlin's solution indicates that slip initially occurs in an annulus having as its outer circumference the boundary of the area of contact. As tangential load is increased, the slip area increases such that the inner annular circumference approaches the center of the circle of contact. Subsequent experiments by Mindlin, et al[10] and Goodman and Brown[11] indicated the validity of this theory. For example, the measured variation of annulus inner radius with the ratio of tangential to normal force was found to agree with theory. Also, the energy dissipation per cycle has been found to agree with theory for a sphere oscillating on a flat[11].

Klint[12] has studied the effects of oscillating forces on contacts formed by crossed cylinders for tangential loads less than required to produce gross slip*. He found that, while even at small amplitudes the behavior was not purely elastic, there is an amplitude of displacement below which no discernable wear occurs even after millions of cycles of

* Gross slip will subsequently be used to designate the situation where the tangential or shear stress exceeds the frictional stress over the entire interface. In the absence of other restraints, large slip deformation or sliding will then occur.

oscillation. At larger amplitudes, wear is rapid and characteristic of fretting corrosion. Measured energy dissipation at amplitudes approaching gross slip was in agreement with theoretical values, but agreement was poor at lower amplitudes. Klint's investigation suggests that the nature of the interactions at the contact surface can be more complex than Mindlin's theory indicates.

It is obvious that interface damping in joints is closely related to such phenomena as friction, adhesion, wear, and fretting of contacting metal surfaces. These phenomena are known to be influenced strongly by environmental factors such as high vacuum.

Because of the vacuum around a joint exposed to space environment, the usual gases, nitrogen, oxygen, carbon dioxide, and water vapor, will be in very short supply. The lack of oxygen and water vapor should have a greater effect on interface damping than the lack of nitrogen or carbon dioxide. Oxygen is very reactive with most metals, and, when it is present, protective oxide coatings form within seconds after exposure of the bare metal. Water vapor similarly participates in many metal reactions, resulting in the formation of a surface coating. Of course, all the gases mentioned above, plus others, may adsorb on metal surfaces and thereby affect surface phenomena. The major results of all of these oxides, films, and adsorbed gases is the lessening of metal-to-metal contact, reduction in seizure of surfaces, and frequently, reduction in friction. In space, the metal surface in a joint cannot acquire any appreciable replenishment of its protective films, and, once these are worn off, the chance of metal-to-

metal contact increases and high friction, seizure, or cold-welding may result.

References describing high friction and seizure of metals in vacuum are very numerous and only a few of particular interest will be cited here. In experiments cited by Bowden and Tabor[13], thoroughly outgassed metal specimens in vacuum had friction coefficients of 5, 6, and 9 for copper-on-copper, nickel-on-tungsten, and nickel-on-nickel, respectively. Correspondingly high values of friction coefficients for metals in vacuum have been reported in a number of more recent investigations.

For example, in an investigation by Brown and Burton[14] the friction coefficient of copper in vacuum (5×10^{-10} to 4×10^{-7} torr) was observed to range from around 2.2 at -270°F to over 16 at 1000°F. Marked cold-welding was observed in these experiments, and measured adhesion coefficients were generally about one-tenth of the friction coefficient under comparable conditions.

Buckley, Swikert, and Johnson[15] report that 52100 steel sliding on itself in a liquid-helium cryogenic pumped vacuum had a gradually increasing friction coefficient for 30 minutes, immediately after which friction coefficient increased abruptly to over 5 and the specimens welded together.

In the three investigations just cited, procedures and conditions were such as to eliminate adsorbed surface films by very careful cleaning of specimens, high temperature outgassing, or by the combination of frictional heating and cryogenic pumping, as in the last investigation cited.

When less stringent outgassing procedures were deliberately used[16] in studies of the frictional behavior of metals during exposure to conditions simulating those on a synchronous satellite, greatly different frictional behavior was observed. In experiments at room temperature and at pressures down to 10^{-9} torr, the friction coefficients of ten metal combinations varied, generally, as follows: friction coefficients were in the range of 0.4 - 0.5 after 1-2 days, rising to about 0.7 - 0.8 after 30 days, and gradually increased to around 1.0 at 200 days vacuum exposure.

The increases of friction in a space environment are due to the loss of various surface films such as oxides, adsorbed gases, and other contaminants. The rate of loss of contaminants and adsorbed gases is governed by the volatility of the substances involved and by the degree of communications with the space environment. Contaminants trapped within a structural joint must escape through the very narrow and tortuous passages in the joint. Rate of loss through such passages will be governed by the mechanism of "molecular flow", which results when the mean free path of the molecules is greater than a characteristic dimension of the passage, for example, the diameter of a tube.

Using arbitrary, but reasonable assumptions, a rough idea of the time required to deplete the air in a joint and of the time required to deplete a film of contaminant can be calculated. We assume that the interstices of a joint are not interconnecting, communicate with the space environment, and are in cross section a circle of diameter approximately equal to twice the average height of surface asperities. Finely turned, shaped, or milled

surfaces could have asperities of around 16 microinches in height. This would provide passages of 8×10^{-5} cm in diameter. The loss rate through such a capillary can be calculated using the following equation[17]:

$$F = 30.48 \frac{a^3}{L} \frac{T}{M}^{1/2} \text{ liters} \cdot \text{sec}^{-1}$$

where

a = radius, cm

L = length, cm

T = temperature, °K

M = molecular weight

If we assume that L is one cm, T is 293°K, and M is 30, we get the following flow rate:

$$F = 30.48 \frac{(4 \times 10^{-5})^3}{1} \frac{293}{30}^{1/2} = 1.15 \times 10^{-12} \text{ liters} \cdot \text{sec}^{-1}.$$

The variation of pressure with time in such an interstice can be calculated as follows:

$$P = P_o \exp\left(-\frac{Rt}{V}\right)$$

where

P_o = pressure at which molecular flows start, assumed here to be 1 torr

t = time in seconds

R = loss rate, 1.15×10^{-12} liters · sec^{-1}

V = volume of interstice

Therefore,

$$P = \exp\left(-\frac{1.15 \times 10^{-12} t}{5 \times 10^{-12}}\right) = \exp(-0.23t)$$

and the pressure will drop to 2×10^{-10} torr in 100 seconds. This result probably represents a minimum for the time required to evacuate joint interstices. In practice, the interstices would be very crooked and flow would be further restricted. The calculation does indicate that air would not be retained in a joint interstice for any significant length of time—provided that the interstice did not connect to a large reservoir of air within the joint.

It is not possible to accurately predict the life of contaminant and adsorbed films on joint surfaces since the composition of the films and the joint interstice configurations are not known in advance. Adsorbed gases and the monolayer of contaminant next to the metal are extremely hard to desorb. References on friction of metals in vacuum, cited earlier, show that this last trace of adsorbed matter is very effective in reducing friction.

It is informative to calculate the life of selected films in a joint interface of one square inch area. Assuming a 50 Angstrom thick layer on each surface, and density of unity, the weight of contaminant is 6.45×10^{-6} gm. Within the joint, it can be assumed the vapor pressure of the contaminant prevails. The loss rate is determined by the area of the peripheral crack. Assuming the crack is 8×10^{-5} cm wide, the resulting area is 8.1×10^{-4} cm^2.

The film life of a low vapor substance, such as Octoil, will give some indication of the approximate life of a thin-oil film. The equation used is as follows:

$$\text{Time} = \frac{\text{Weight of Contaminant}}{\text{area x evaporation rate}}$$

$$= \frac{6.45 \times 10^{-6}}{8.1 \times 10^{-4} \times 0.66 \times 10^{-8}}$$

$$= 1.2 \times 10^{6} \text{ sec or } 13.9 \text{ days.}$$

This result is useful principally to give some idea of the minimum duration of vacuum tests and to show that the life of a thin-oil film in a joint is probably best measured in days rather than months.

Several surface factors have a significant effect on friction, adhesion, and fretting of metals in contact. These phenomena will all be involved in interface damping in joints. Surface factors anticipated to be of significance in this program include presence of contaminants and adsorbed gases on surfaces, presence of oxides or other surface chemical compounds, roughness and texture of surface, and the degree of work hardening.

The role of contaminants and adsorbed gases in reducing friction and adhesion of metals was just discussed. Aside from the cleaning effect of vacuum exposure, the degree of initial surface cleanness can be a major factor affecting interface damping. Extremely clean surfaces should provide results indicative of the ultimate effect of the space environment on damping. However, "commercially clean" surfaces—cleanness which

could be achieved and maintained on surfaces of large metal components—might be more indicative of damping in actual joints.

Oxide films and other compounds attached lightly or loosely to the surface can have significant effects on interactions. All of these compounds tend to impede metal-to-metal contact and reduce welding and friction in most instances. The protection afforded by these films depends on factors such as relative hardness of film and substrate, strength of bonding, shear strength of the film, film thickness, and roughness. Soft, thick films provide low friction. Hard, thin films are easily cracked, and this tendency is accentuated where films cover rough surfaces[18]. As an example, aluminum oxide is very hard, 1800 kg mm^{-2} [18] as compared to 60 kg mm^{-2} for 7075 soft aluminum and 150 kg mm^{-2} for 7075 aluminum in T-6 condition. Aluminum oxide also has a friction coefficient around 0.8 according to Whitehead[19] who reports the friction coefficient of bare aluminum on itself as 1.2.

Surface topography may also have an effect on interface damping. The height, shape, and distribution of surface asperities play a major role in establishing area of real contact and size, number, and shape of voids between the surfaces. With increasing roughness, area of real contact for a given load decreases slightly[20, 21] and volume of void increases[21, 22]. These two conditions would provide for more rapid loss of contaminants from the joint surfaces than in the case of smoother surfaces. The lifetime of harder, thin, surface oxide layers subject to mechanical wear can be

influenced by the effect of surface topography on the local stress distribution at the points of contact.

The bulk properties of the contacting solids also play a role in interface phenomena. Relevant bulk properties are modulus of elasticity, hardness, yield strength, shear strength, internal damping capacity, and work hardening characteristics. When solids are brought into contact, the real area of contact is determined by modulus of elasticity, hardness, yield strength, and work hardening capacity, in addition to surface geometry.

The area of real contact has generally been considered to be primarily a function of hardness. For example, Bowden and Tabor[13] have reported that area of real contact is inversely proportional to the mean yield pressure of the asperities or, practically, to the indentation hardness measured in pressure units. Materials which are susceptible to work hardening will have an area of real contact slightly less than that indicated by the load hardness ratio. Greenwood and Williamson[23] point out that this dependence of area of real contact on hardness is applicable to initial loading but that in subsequent loadings the elastic properties must play a significant role in establishing area of real contact. In fact, their results show that area of contact is inversely proportional to the two-thirds power of modulus of elasticity when the number of contacts remains constant and that when the mean size of asperity contacts is constant the area of contact is inversely proportional to the elastic modulus.

Based on the discussion of the preceding paragraphs, a qualitative description of the phenomena occurring at a joint interface can be constructed.

When the joint surfaces are brought together, a few points contact initially and as the load increases the number of points in contact increases. Except at very heavy loads, both plastic and elastic contacts exist. Upon the application of a tangential force, additional plastic deformation will occur at the plastic contacts, resulting in an increase in area of real contact. As the tangential force increases, a level will be reached at which local slip at individual junctions occurs or, at sufficiently large loads, actual shearing of asperities may occur. With continued oscillatory loading, a steady state condition will develop in which most of the contacts have been work-hardened to the point where they are essentially of the elastic type. At the steady state condition the area of real contact would remain relatively constant. Thus, in the early stages of the loading, energy may be dissipated by plastic working of highly loaded asperities and even shearing failures for sufficiently large motion. Under continued oscillary loading, a steady state condition must result in which the primary energy dissipation arises from the continuous making and breaking of surface bonds at the localized areas of contact under the action of the shear loading.

In the case of oxide covered metals, bare metal contact might increase with continued vibration of the joint due to mechanical rupture or fatigue causing attrition of the oxide. The degree of energy dissipation in the joint will be affected by this growth of metal-to-metal contact, since the bonding energy (and coefficient of friction) is different between the oxide and the base metal. Accompanying rupture and attrition of oxides will be the formation of wear particles between the surfaces. These particles may remain loose,

and if trapped between surfaces, could appreciably affect the mechanical behavior of the joint. The influence of surface oxide layers on the mechanics, particularly the energy dissipation, in joints will depend upon the relative properties between the specific metal and its oxide. We might expect quite different behavior from a metal with a hard oxide such as aluminum than from a metal such as iron whose oxide is relatively soft. It is anticipated that differences between interface damping tests performed in air and in vacuum can be largely governed by the attrition of surface oxides. This appears to be born out by the subsequent experiments.

The problem, then, involves complex surface mechanics and surface reactions with many interacting parameters. The following experiments were designed to hopefully clarify at least some of the mechanisms involved.

EXPERIMENTAL PROGRAM

Considerable consideration was given to the type of experiment which could provide the most qualitative and quantitative insight into the mechanics of the interface damping phenomena. As discussed in the preceding section, previous experiments have been conducted with simulated structural elements, primarily beams[3,4,8], or specimens with small relatively well defined contact areas of the Hertzian type[10,11,12]. Experiments with beams provide a reasonable simulation of actual practice while maintaining a geometry which is analytically tractable. However, the configuration is not suitable for easy control and variation of the loading and interface surface parameters. For vibrating beams, the additional effects

of air drag damping must also be accounted for in comparisons between vacuum and atmospheric tests. On the other hand, experiments with small spheres or cylinders characteristic of friction experiments, while being better defined in terms of the distribution of normal load, do not provide simulation of the mechanics of the continuous interface characteristic of structural joints. The limited contact area does not provide for the entrainment of wear products and other mechanical effects suspected to be important in the continuous interface.

The specimen configuration chosen represents a compromise. It consists of two, nominally flat surfaces held together with uniform normal loading and subject to oscillatory loading tangential to the interface. The nominal area of contact is one square inch. The tangential force and displacement are measured as continuous functions of time or as the force-displacement hysteresis loop in order to determine the energy dissipation per cycle of oscillation.

For this system, we define two ranges of the loading parameter, $F_t/\mu N$, where F_t is the peak oscillatory tangential force, N is the constant normal force, and μ is the coefficient of Coulomb friction for the interface. If $F_t/\mu N < 1$, the deformation will be referred to as "microslip". In this range the relative displacements between the two sides of the interface must be accommodated by elastic displacements in the bulk material. This region is characterized by increasing slip area with increasing tangential force. The applied tangential force results in a distribution of shear stress which is non-uniform over the interface, having a maximum at the two boundaries

which are perpendicular to the direction of the applied force. The stress distribution is similar to that in a lap joint[24]. Slip is initiated at the two boundaries and moves progressively toward the center of the specimen with increasing applied tangential force. For the specimen dimensions used in the present experiments, the microslip displacements will be small compared with the dimensions of the surface roughness or distance between surface asperities. The amplitude of the oscillatory displacement relative to the asperity dimensions is important with respect to the degree of surface damage that can be produced by the motion.

When the tangential force exceeds the frictional force, $F_t/\mu N > 1$, gross slip will occur. In this region the two specimens move as rigid bodies with respect to each other and arbitrarily large relative displacements may be produced. We should, therefore, expect more surface damage to occur in the gross slip region as the surface asperities will be sliding over one another. The hysteresis loop will be similar to Figure 1b. The boundary between the two regions, $F_t/\mu N = 1$, defines the coefficient of friction, $\mu = F_{t_o}/N$, where F_{t_o} is the minimum tangential force required to initiate gross slip or sliding for a given normal force. It should be noted that μ is defined only with respect to the load parameters but will be a function of the surface and environmental parameters also. The coefficient of friction may vary widely with changes in these other parameters and also with time if surface conditions are changing.

The following parameters are of interest in this study:

Load Parameters

1. Static normal force
2. Oscillatory tangential force

Surface Parameters

1. Substrate material properties (elastic, plastic, thermo-physical, chemical)
2. Roughness
3. Cleanness

Environmental Parameters

1. Gas pressure
2. Gas composition
3. Temperature
4. Time of exposure to test.

Interface Damping Apparatus

The apparatus used in the reported experiments is shown in Figures 2a and 2b. It provides for a two-specimen, single-interface configuration. One specimen is rigidly supported and the other is oscillated in a vertical direction by the permanent magnet exciter. Normal load is applied by weights acting through a load cable and a crank. The driven specimen is carried on the vertical drive rod and is free to align itself in one plane against the stationary specimen by virtue of the two bending flexures in the driven specimen support system. The driven specimen holder is rotated about the vertical axis to provide initial specimen

alignment in the other plane and then is locked in position. Further, small misalignments can be accommodated by virtue of a torsional flexure between the drive rod and the driven specimen support.

Tangential driving force is measured by strain gages mounted on a reduced section of the drive rod. Relative displacement between the two specimens is measured by a high resolution, non-contacting type displacement probe mounted on the stationary specimen and referenced to an aluminum block mounted on the driven specimen as shown in Figure 2b. Force and displacement signals are displayed on a Tektronix type 536 oscilloscope, with force on the vertical axis of the oscilloscope and displacement on the horizontal axis. Each signal may also be displayed individually as a function of time.

Since the applied tangential force is transmitted entirely by the shear or frictional forces at the specimen interface* and the displacement is relative displacement directly across the interface, the area within the displayed force-displacement hysteresis loop represents the energy dissipated at the interface during one cycle of oscillation. The hysteresis loops are photographed as necessary to provide permanent records of the experimental data.

The strain gage force transducer and the displacement probe were both calibrated at one atmosphere and at approximately 10^{-9} torr vacuum. The calibration constant for each transducer was found to be unaffected by

* The normal load is applied through a pin which is free to rotate and thus cannot provide reaction to the tangential force.

the environment, assuring that the measured quantities represent changes at the interface and not in the measuring system.

Friction Rig

In a few experiments, concurrent with the interface damping measurements, friction experiments were conducted on a crossed-cylinders friction rig mounted on a flange opposite to the interface damping apparatus. The friction rig is shown schematically in Figure 3. A cylindrical-vertical specimen, having 1/2-in. diameter and carried by a gimbal-mounted arm, is oscillated while in contact with a cylindrical-horizontal specimen, having 1/2-in. diameter and held by a stationary arm. Wear track length is approximately 37 cycles per minute. The present experiments were run at 20 cycles per minute. Normal load is applied by dead weights pulling on the gimbal-mounted arm through a cable and pulley. Normal loading of 4 lbs was used in most experiments. The normal load is indicated by two strain gages mounted inside the stationary tubular arm, while another two strain gages mounted in the same tubular arm indicate friction force. Signals from the friction measuring strain gages were fed to an oscilloscope.

The friction specimens were fabricated from the same bar of 7075-T6 aluminum from which the interface damping specimens were fabricated. Cleaning procedures were identical to those used for the interface damping specimens.

Vacuum Equipment

The tests were conducted in a 24-inch diameter x 60-inch long stainless steel vacuum chamber which has a 6-1/2 cubic foot test volume. A 1200 liter/second ion pump is built into the walls of the chamber around the periphery of one end. The ion pump plus a titanium sublimation pump provide a combined pumping capacity of 22,000 liter/second.

Rough pumping is provided by a 100 cfm Heraeus two-stage blower backed with a 15 cfm Welch mechanical pump. Back streaming of mechanical pump oil is prevented by a 2-inch diameter molecular sieve trap between the blower and the ultrahigh vacuum valve to the chamber. Pumpdown is very rapid with this system. In less than 8 minutes, chamber pressure of 5 microns or less is attained and the ion pump can be started.

Without bakeout, chamber pressure of 5×10^{-9} torr can be obtained in two hours. Following an overnight mild bakeout, chamber pressures of less than 1×10^{-9} torr were attained at room temperature. Pressures are measured with a nude hot cathode ionization gage which measures pressures down to 2×10^{-11} torr.

In addition to the hard vacuum, experiments were conducted at atmospheric pressure (760 torr) with dry air (dew point - 75°F), high purity dry nitrogen (99.995% minimum purity), and high purity argon (99.996% minimum purity). In these experiments the chamber was purged three times with the test gas by evacuating the chamber to a pressure of less than 5 microns and then back-filling it to atmospheric pressure.

Specimen Data

A pair of identical specimens having a nominal contact area of one square inch was used in each interface damping experiment.

Only one specimen material, 7075-T6 aluminum was used in these experiments. This material was received in the form of three bars, 1/2 inch x 1-1/2 inch x approximately 12 feet. Chemical analyses and hardness measurements shown in Table 1 indicate that all three bars are within the composition limits for 7075 aluminum and that the hardness is generally within the range of $85R_B$ to $95R_B$ as specified for the T6 heat treat condition. All specimens were in the T6 heat treated condition.

Properties of 7075-T6 aluminum[25], used in latter calculations, are as follows:

Elastic modulus:	10,400,000 psi
Modulus of rigidity:	3,900,000 psi
Poisson's ratio:	0.33
Yield strength:	73,000 psi

Surface Preparation

Early in the program, surfaces prepared by abrasive blasting and by machine lapping were evaluated. These techniques were discarded because of embedded abrasive particles in the first case and because of lack of parallelism between clamping surface and test surface in the second case. All the specimens used in experiments reported herein were finished with a single-point flycutter on a milling machine. The flycut surfaces

provided a more uniform distribution of contact area when two specimens were mated. This avoided the occurrence of "rocking" on a single contact point which was encountered with the abrasive blasted or lapped surfaces. The only disadvantage of the flycut surface is that it does have directional properties. Machining data were: cutter speed 660 rpm, feed 0.937 in/min, cutter diameter 1.75 in., and tool nose radius 0.015 in. The resulting surface finish consisted of curved ridges at a nominal spacing of .0014 inches. A typical surface profile at 90° to the ridges is shown in Figure 4a. The roughness of these surfaces was in the range of 15-20 microinches CLA.

TABLE 1. COMPOSITION AND HARDNESS OF 7075-T6 ALUMINUM SPECIMEN MATERIAL

Element	Bar No. 1	Bar No. 2	Bar No. 3
Chromium	.23%	.24%	.22%
Copper	1.63	1.51	1.55
Iron	.25	.27	.24
Zinc	6.00	5.82	6.00
Magnesium	2.61	2.61	2.61
Silicon	.12	.13	.13
Manganese	.05	.05	.05
Titanium	.01	.01	.03
Others Each	*.05	*.05	*.05
Others Total	*.15	*.15	*.15

* less than.

Hardness (Average)	$87R_B$	$93R_B$	$89R_B$

The specimens were machined so that surface contact occurred at approximately 90° between ridges in the experiments. The orientation of ridges on mating surfaces is shown in Figure 4b.

For all tests reported herein, specimens were cleaned by the following procedure:

(1) Vapor degreasing in trichloroethylene

(2) Immersion for three minutes in caustic solution (8 gm sodium carbonate, 6 gm trisodium phosphate, and water to one liter) at 170-200°F.

(3) Rinsing with hot water

(4) Immersion for three minutes in acid solution (60 gms chromic acid, 160 cc sulfuric acid, and water to one liter) at 110-180°F.

(5) Rinsing with hot water.

Surfaces cleaned by this technique were sufficiently clean to be "wet" by water.

Experimental Procedures

Most of the experiments discussed herein, consisted of three parts: short-duration microslip runs at increasing tangential force, a long-duration microslip run, and 4-hour gross slip run. After the desired ambient atmosphere had been attained the sequence of runs for a single specimen was normally as follows:

(1) A series of 10-minute microslip runs was made at progressively increasing tangential force up to $\pm$ 15-lbs which was below the force required

to cause gross slip. Other experimental conditions were 20-lb normal load and oscillation at 50 cps. At the end of each 10-minute run, the hysteresis loop was photographed. This provided data for measuring the compliance and energy dissipated.

(2) A long-duration (up to 72-hr) microslip run was made at 50 cps, 20-lb normal load, and at $\pm$ 15-lb tangential force. Hysteresis loops were photographed intermittently during this run.

(3) Another series of microslip runs was performed. This was identical to the series described under item (1) except that the runs were continued to higher tangential forces. The results from this series could be compared with series (1) to show possible effects of the long-duration microslip.

(4) A 4-hr duration gross slip run was made at 12 cps, 10-lb normal load and at whatever tangential force was required to maintain gross slip.

(5) Finally, a series of short-duration microslip runs was made. This series was identical in all respects with the series described under item (3) above. This series could again be compared with series (1) to show effects of gross slip on subsequent microslip behavior.

In all the experiments described above, the principal source of data was the force-displacement hysteresis loop. In several experiments, additional data was obtained from photographs of oscilloscope traces of force, displacement, and velocity, all versus time.

The experimental procedures were varied in several experiments, but details of the departures from the usual procedures will be described where the data involved is being presented. There was no apparent effect of frequency within the range of 12 to 50 cps utilized.

EXPERIMENTAL RESULTS

Surface Observations

For surfaces maintained within the microslip range there was little observable surface damage, either in air or in vacuum. For aluminum, the surfaces initially have a hard oxide layer which is present when the specimens are first placed in the test apparatus. For the small tangential forces applied in the microslip range, this oxide layer does not appear to be appreciably disturbed by the localized motion occurring at the interface. There may be, however, some attrition of the oxide layer at localized points of contact and high stress not detectable at the levels of optical magnification used.

Specimens subjected to gross slip exhibited easily detected areas of surface damage as shown in Figure 5. It is observed that gross slip damage incurred in vacuum consists of areas of heavily worked metal which is bright and highly reflective as shown in the upper photomicrograph of Figure 5. Also, after gross slip in vacuum, there are no loose wear particles. Surface damage incurred from gross slip in air, however, consisted of areas of disturbed metal which were black, as shown in the lower photomicrograph of Figure 5. The black areas have fine black particles

worked into the metal and lying loose on the surface. Following gross slip experiments in air, wear debris was always in evidence. Some of this debris is shown in Figure 6 with 60X magnification. It is expected that most of this debris consists of hard oxide particles.

Figure 7 shows that even with small, carefully prepared specimens it is not possible to get uniform contact over the entire surface. Primary contact is made over several localized areas as most easily seen on the specimen tested in air where the black wear debris makes the wear areas visible. Since the height of the asperities or machining ridges are approximately 40 microinches, peak to trough, it would be necessary to maintain all the peaks at the same level to within only a few microinches to produce contacts uniformly distributed over the entire surface under reasonable normal loading. Variations in the detailed distribution of contact area from specimen to specimen undoubtedly accounts for some of the variation in the measured parameters.

Microslip Results

Figure 8 presents a typical microslip hysteresis loop indicating the relative magnitudes of the tangential force, F_t, and the relative displacement, δ. Data taken from loops of this type include the maximum tangential force, $\overline{F_t}$ (1/2 loop height) and maximum displacement, $\overline{\delta}$ (1/2 loop width), and energy dissipated per cycle, ΔE (area enclosed by the loop). In order to facilitate discussion, these data have been plotted in terms of both interface compliance, $C = \delta/\overline{F}$ (displacement/tangential force) and energy

dissipated per cycle versus several independent parameters for both vacuum and air test conditions. Larger values of compliance indicate decreased resistance of the interface to slip and, thereby, smaller values for the effective coefficient of friction. Similarly, at equal tangential force input, an interface with a high effective coefficient of friction will dissipate less energy than an interface with a lower coefficient of friction. For equal slip displacement amplitudes, the converse will hold. The above statements hold true as long as we are restricted to the microslip region.

For the microslip region, results will be presented for both the initial series of tests with the virgin surfaces as well as a similar series taken after the specimen had been subjected to a period of gross slip as outlined under the experimental procedure. This is done in order to illustrate the effect of prior history of deformation of the interface on subsequent behavior. It should be mentioned that the magnitude of relative displacement during gross slip of these small specimens is still within the order of magnitude to be expected in the deformation of a structural joint.

Compliance. Plots of compliance versus force, as shown in Figures 9 and 10*, reveal that during initial microslip runs the compliance in vacuum and in air is nearly constant for tangential forces of up to 15 lbs, which corresponds to roughly 60 per cent of the tangential force required to

---

* The numbers in parenthesis in the Figure captions designate the specimen or run number.

cause gross slip. Careful examination of the compliance data shows that in vacuum the compliance tended to decrease slightly with increasing tangential force and that in air the compliance tended to increase slightly. The plots of Figures 9 and 10 also show that during the initial microslip runs the compliance was about the same in air as in vacuum.

The only significant difference between compliance in air and in vacuum was observed for specimens which had been subjected to gross slip. Compliance versus tangential force are plotted in Figures 11 and 12 for the same specimens as shown in Figures 9 and 10, but after a period of gross slip of approximately four hours. After gross slip in vacuum, compliance decreased to about one-half of its initial value. Following four hours gross slip in air, compliance increased as much as three times.

In vacuum, compliance after gross slip was nearly constant for loads up to approximately 55-lbs which represents a tangential force approximately equal to 0.8 μN. Compliance after gross slip in air tended to increase with increasing tangential force, as shown in Figure 12. The scatter between specimens, always appreciable, was increased significantly by the period of gross slip in air. This increased scatter is attributed to the continuing generation of wear debris during gross slip in air and its mechanical action within the interface.

During the long-duration (72-hr) microslip runs on the virgin specimens, compliance measured periodically during each run remained fairly constant as shown in Figures 13 and 14. Compliance for vacuum runs ranged from 1.1 to 3.25 μ in/lb for the four runs plotted. Compliance

for the runs in air were slightly higher and more scattered, falling in the range from 1.4 to 4.1 μ in/lb. These long-duration runs were made at a constant tangential force of $\pm$ 15 lbs.

Energy Dissipation per Cycle. The results for energy dissipation per cycle* during microslip oscillation in vacuum and air are plotted in Figures 15-18. The tangential force and displacement parameters are peak to peak amplitudes, i.e., measures of the total force and displacement range. Again, as for compliance, results are presented for an initial series of tests on the virgin specimen and for the same specimen after it had been subjected to a period of gross slip.

The linearity of the results when plotted on the logarithmic scale indicate that the energy-force and energy-displacement relations can be expressed by

$$\Delta E = K\overline{F}_t^{\,m} \tag{3a}$$

or

$$\Delta E = K'\overline{\delta}^{\,m'} \tag{3b}$$

where ΔE is the energy dissipated per cycle, K, K', m and m' are constants and $\overline{F}_t$ and $\overline{\delta}$ are the force and displacement double amplitudes during the cycle (peak to peak amplitude). Values of these constants determined from a least squares fit to all the data of each series are given in Table 2. The statistical correlation coefficient for each set of data is also given.

* ΔE is given in units of total energy dissipation (in-lb). However, since the specimen area is 1 in^2, the units will be the same for specific energy dissipation (in-lb/in^2).

The most distinct differences in energy dissipation occur for those specimens which have been subject to gross slip. For these specimens, the areas of contact have been subject to mechanical wear. For the tests in air, wear debris has accumulated in the interface. For the tests in vacuum, the oxide layer has been mechanically removed and metal to metal contact established. After gross slip, the energy dissipation in air is greater than in vacuum for equal force input (compare Figures 15b and 16b). For the same situation, the dissipation is less in air than in vacuum for equal displacement (Figures 17b and 18b).

For the initial runs with the virgin specimens the differences in energy dissipation are not as great. For both the air and vacuum runs, the interface is probably controlled by the oxide layer with only microscopic wear occurring. Comparing the "initial" and "after gross slip" results in Figures 15 and 16, it is seen that the period of gross slip caused an increase in the energy dissipation in air and a decrease in the dissipation in vacuum at equal force amplitudes. Curiously, at low force amplitudes the mean curve for energy dissipation in air is somewhat greater than that for the vacuum tests. It is not certain that this is a real or significant difference.

The equations (3a) and (3b) are related through the compliance, C, such that

$$C = \frac{\bar{\delta}}{\bar{F}_t} = \left(\frac{K}{K'}\right)^{\frac{1}{m'}} \cdot \bar{F}_t^{\left(\frac{m}{m'} - 1\right)} \qquad (4)$$

This relation shows the compliance to be amplitude dependent. From Table 2, it can be seen that $\frac{m}{m'}$ is less than one for the vacuum tests and greater than one for tests in air. This is in agreement with the compliance decreasing with force amplitude in vacuum and increasing in air, noted in the preceding section.

The change in energy dissipation during 72 hour runs in air and vacuum for constant load conditions is shown in Figures 19 and 20. During this period of three days there does not appear to be any major change in the behavior, either in air or in vacuum.

TABLE 2

Values of K and m from Microslip Tests in Air and Vacuum With Correlation Coefficients for Each Set of Data

		$\Delta E = K F_t^m$			$\Delta E = K' \delta^{m'}$		
		m	K	Corr. Coef.	m'	K'	Corr. Coef.
Vacuum	Initial	1.85	0.352	0.904	2.18	0.034	0.953
	After Gross Slip	2.24	0.037	0.739	2.60	0.011	0.968
Air	Initial	2.31	0.049	0.787	1.92	0.043	0.968
	After Gross Slip	2.71	0.032	0.838	2.16	0.013	0.856

Gross Slip Results

Gross slip data includes hysteresis loops from four hour runs made in air and in vacuum, from shorter duration runs made in selected

gases (dry air, nitrogen, and argon), and from runs conducted over a range of atmospheric pressure.

Hysteresis Loop Characteristics. Hysteresis loops for gross slip are shown in Figure 21. The maximum displacements are of the order of a few thousandths of an inch with the two blocks sliding essentially as rigid bodies. In gross slip there is an appreciable difference in the shape of the hysteresis loop between air and vacuum. In vacuum, the loop is rectangular with the slip motion being maintained by nearly constant tangential force. In air, gross slip is initiated at a relatively low load, but the frictional force increases with displacement. The lower two loops of Figure 21 show the existence of oscillations produced by stick-slip action at the interface coupled with the elasticity of the driving system. Since the stability of the driving rod is involved, the oscillations are more prevalent on the push or compression half of the cycle than on the pull or tension half. The stick-slip oscillations were the exception rather than the rule and may have been influenced by slight initial misalignment of the specimen.

The rectangular shape of the gross-slip hysteresis loop in vacuum is that to be expected based upon classical Coulomb friction if the static and kinetic coefficient of friction are equal and constant. Thus, when the increasing tangential force reaches the critical frictional force (μN), slip is initiated and continues under this constant force until the direction of loading is reversed. Most of the loops obtained in these experiments had somewhat rounded corners.

Difficulty was encountered in attempting to stabilize the gross slip loops in vacuum. Since the electromagnetic shaker is force controlled rather than displacement controlled, once slip occurs small changes in force input or change in frictional resistance of the interface can cause large changes in the displacement. This problem was not as severe with the air tests because of the positive slope to the force-displacement relation during slip in this condition.

In two experiments, pressure was slowly increased from the vacuum condition by bleeding dry air into the chamber while the specimens continued to oscillate in gross slip motion. It was observed that at a pressure of approximately 0.1 torr, the hysteresis loop abruptly changed from the nearly rectangular loop to the parallelogram shape characteristic of gross slip oscillation in air. The initial change was to the form of the loop at the bottom right of Figure 21, but as oscillation continued the loop began to harden sharply at the end of the stroke as in the upper right of Figure 21. In other experiments, where gross slip oscillation was started in air at atmospheric pressure, a similar initial parallelogram loop shape and subsequent loop hardening with continued oscillation were observed. At present, our supposition is that the shape of the loop in air is governed by the action of the wear particles accumulating with time in the interface. These particles may either roll or plough into the surface producing mechanical action quite different than pure slip. The hardening at the end of the stroke may be due to the pile up of particles at the end of the wear track causing increasing resistance to the motion.

In order to provide additional evidence to the effect that the primary difference between the results obtained in air and in vacuum is a result of the presence of oxygen in the atmosphere rather than of the gas pressure itself, several tests were run with pure nitrogen. For tests started in vacuum and subsequently admitting nitrogen slowly into the chamber, there was no marked change in loop shape as the pressure reached one atmosphere. However, while the initial loop characteristics in nitrogen were similar to those in vacuum, as oscillation continued there developed a rather curious change in loop shape. Gross slip hysteresis loops in nitrogen after 30 seconds and 1 hour of oscillation are shown in Figure 22. We can think of no obvious reason for the development of such a saddle-shaped loop, as one would not expect nitrogen to react with aluminum to any extent at this temperature. If, for the same specimen, the nitrogen was subsequently replaced by air, the hysteresis loop shape characteristic for air was recovered.

Force, Displacement, and Velocity Relations. In several experiments, force, displacement, and velocity versus time were displayed on the oscilloscope and photographed in order to show the phase relations between these parameters and to relate them to the unusual shape of the hysteresis loops for gross slip in air.

A set of these oscillograms for gross slip oscillation in air are shown in Figure 23. The upper oscillogram is a typical hysteresis loop for gross slip oscillation in air. The lower oscillogram records show

the displacement, velocity and force as functions of time on the horizontal axis. Scales for each trace are shown. All three oscillograms were taken from the same specimen within a few minutes. Corresponding points on the hysteresis loop and the time traces are numbered. The oscillograms show that maximum velocity during sliding was 0.36 in/sec and that the average acceleration was 60 in/sec^2.

As also indicated by the hysteresis loop, the time histories show that tangential force continues to increase after slip is initiated and reaches its maximum after slip has essentially stopped. It is interesting to note that slip occurs during only a small portion of the total period of oscillation.

Energy Dissipation per Cycle. Energy dissipation per cycle versus peak to peak displacement for vacuum and air runs is plotted in Figures 24 and 25. In gross slip the vacuum results show significantly greater energy dissipation in vacuum than in air for equal displacement amplitudes. The energy dissipation per cycle is, of course, much greater than in the microslip region.

While the shape of the gross slip hysteresis loop is quite different when obtained in vacuum and in air, in both cases the energy dissipation increases very nearly linearly with displacement. The slope of the straight lines drawn in Figures 24 and 25 is unity. The linear relationship is an obvious consequence of a rectangular hysteresis loop, as obtained in vacuum. The linear relation appears to hold also for the non-rectangular hysteresis loops from the air tests.

Although, after gross slip is established, the energy dissipation at constant amplitude is greater in vacuum than in air, it requires a greater tangential force to initiate gross slip in vacuum. This difference may be as much as a factor of two (see Figure 21) and will be evidenced in the relative magnitudes for the effective coefficient of friction between the two conditions as presented in the next section.

As previously pointed out, an additional effect evidenced in the vacuum tests was the instability of the hysteresis loop. Under constant running conditions the loop would often close up, due either to slight fluctuations in the amplitude of the exciting force or, more likely, to increased frictional resistance of the joint interface. Since the force-displacement relation is very flat after slip has been initiated in vacuum, small changes in the exciting or resisting force produce large changes in displacement.

Figure 26 shows one run at a constant 10 lb. normal force where it was possible to obtain continuous data in the microslip and gross slip range. The change in slope occurs at the transition from microslip to gross slip. This transition occurs at $F_t = \mu N$.

Coefficient of Friction

The coefficient of friction was obtained from two sources: the gross slip interface damping experiments and the crossed-cylinders friction rig described in Figure 3.

Coefficients of friction during gross slip oscillation of five specimens in vacuum are plotted in Figure 27 as functions of time. The

coefficient is based upon the maximum tangential force during slip and the normal load. For vacuum the maximum force and the breakaway force to initiate slip are nearly the same. Results for the coefficient of friction obtained from the interface data taken in air, however, differ significantly depending upon whether the maximum force or force to initiate slip is used. Coefficients determined both ways are plotted in Figure 28. The breakaway coefficient of friction in air is seen to be approximately 0.5, or less than one-half of the average value of 1.25 obtained in vacuum or of the value based upon maximum tangential force in air. In all cases there did not appear to be any significant change in coefficient during the four hours of oscillation.

Simultaneous with two experiments in dry air and one in vacuum, friction experiments were performed on the crossed-cylinders friction rig. Specimens were identical 7075-T6 aluminum as used in the interface experiments. Friction forces were measured intermittently during the experiments which were up to 85 minutes duration. A normal load of four pounds was used and an oscillation rate of 20 cpm with a stroke of 5/16 inch. Average friction coefficients of 0.83 and 0.70 were obtained in air and in vacuum. These values fall between the values obtained from the interface experiments and appear more insensitive to vacuum effects.

At this point, the amount of friction coefficient data from the friction rig is too limited to permit any attempt at correlating it with the friction data from the interface damping experiments. The differences in friction coefficient do indicate the danger in applying friction coefficients

obtained in one experimental condition to a different experimental condition. Several major differences between the two experimental conditions are worthy of mention. The contact stresses may be very different between the case of two 1/2-inch diameter cylinders in contact at right angles and the case of two 1-inch square nominally flat surfaces. Sliding speeds are significantly different in the two cases: in gross slip damping experiments at 12 cps and 0.004-inch displacement, the average speed is 0.048-inch per second; whereas, in the friction experiments at 20 cpm and 5/16-inch displacement, the average speed is 0.21-inch per second. The contact conditions differ in another respect. In the case of the damping experiments, the asperities of the contacting surfaces are potentially in contact all of the time; but in the sliding friction experiments, the asperities on one of the specimens are in contact with the other surface only intermittently.

DISCUSSION

The results presented illustrate the complex nature of the energy dissipation in joints subject to oscillatory sliding contact. The essential feature of the problem is the determination of the effective resistance of the joint interface to tangential or shear forces. Problems of this type are generally treated upon the assumption that the interface shear stress is governed by the action of Coulomb friction, whereby the tangential force necessary to produce relative displacement at the interface is directly proportional to the force normal to the interface. The proportionality

constant is the coefficient of friction. While this coefficient is explicitly defined with respect to the load parameters, it is also a function of the geometry of the interface, the surface and material properties, and other environmental effects such as pressure and temperature. Thus, while the concept of the shear stress at an interface controlled by Coulomb friction has been found satisfactory to describe the behavior of a wide range of specific joint configurations ranging from continuous beams to Hertzian type point contacts, explicit values for friction coefficient are generally determined empirically for each specific situation.

In discussing the present results, it is also convenient to describe differences between tests in terms of changes in the effective coefficient of friction for the interface.

The primary differences in the present tests between specimens run in vacuum and in air environment appear to be due to the presence or absence of oxygen and the depletion or replenishment of the surface oxide layer during oscillation. The oxide of aluminum is harder and has a lower coefficient of friction than the base metal. The coefficient of friction for aluminum oxide is 0.8, while for bare aluminum it is 1.2[19]. The oxide layer on aluminum is very thin so that it may be broken up under the action of surface tractions. For small tangential forces and displacements, as occur in the microslip range of the present experiments, there is little apparent surface damage or breakup of the surface oxides. In microslip, there was no indication of any macroscopic oxide particles formed in the interface. Differences, therefore, between test results for initial microslip

runs in air and in vacuum were small, with only slight indication that the coefficient of friction may be higher in vacuum than in air becoming evident at the higher microslip amplitudes.

For the relatively long duration microslip runs of up to three days (72 hours), there was a slight tendency for the vacuum tests to indicate an increasing coefficient of friction while the air tests did not show much change. For the duration (13×10^6 cycles) and the loading ($F_t/\mu N \approx 0.9$) used, these changes were not large. At the asperities where contact is made, a contact fatigue situation exists which might lead to failure of the surface oxide layer with time. In vacuum, if the oxide is removed at the points of contact, it cannot be replenished and metal to metal contact is established with an accompanying increase in adhesion forces and coefficient of friction. For the same situation in air, the oxide is continuously replenished and the properties of the contacting surfaces are relatively constant with time.

If the relative displacements of the interface become large enough to actually move asperities across one another and produce shearing failures in the hard oxide layer and even in the base metal, the differences between vacuum and air runs become more apparent. Such is the case when gross slip occurs. The gross slip damage is readily visible as shown in the micrographs of Figure 15. If the large displacements and surface damage occur in vacuum, large areas of metal to metal contact are established and the resistance of the interface to deformation is increased, again because of the higher friction coefficient of the base metal. This damage occurs in

the first few cycles and is not a fatigue process. If the gross slip is occurring in the presence of oxygen, the oxide is continuously removed and replenished almost immediately. This results in a continuous generation of oxide particles or debris which remains trapped in the interface. These hard oxide particles tend to reduce the shear resistance of the interface for small displacement amplitudes. This is indicated by the increased microslip compliance of specimens tested after gross slip had occurred and by the much lower tangential forces required to initiate gross slip in specimens tested in air. At increasing displacement amplitudes in the gross slip region, however, the mechanical action of the oxide particles provides an increasing resistance to slip. This may be caused by increased plowing action by the particles, by increased interaction between particles in a wear track, or by some other unknown mechanism. The gross slip hysteresis loop in air shows continuing hardening with time which would appear to be associated with the continuous generation and therefor increase in the total amount of debris present. The increasing resistance to slip after gross slip has been initiated in the air tests differs from classical Coulomb friction where the kinetic coefficient of friction remains constant.

The gross slip results in vacuum did exhibit a nearly constant shear resistance during slip, with an effective coefficient of friction near to that reported for bare aluminum. Seizure often occurred in the gross slip vacuum tests, with small increases in the shear resistance of the interface causing the displacements to suddenly decrease to small microslip values. This type of instability should be characteristic of sliding surfaces in vacuum.

A few tests run in the other gases tended to support the conclusions regarding the important role of oxygen. However, both nitrogen and argon also produced some unusual gross slip hysteresis loops, indicating some reaction of these gases with the surface. Structures operating in other atmospheres than air may have to be tested in that atmosphere. Water vapor was removed from the air in the present tests, but it too may effect the parameters studied.

Surface cleanness is another parameter which is very important and was carefully controlled in the present tests. Just a fingerprint can alter the results drastically. However, such low vapor pressure contaminants will be removed upon sustained operation in vacuum as indicated in the preliminary discussion. Frequency and temperature effects were not investigated to any extent. Over the frequency range available, 5 - 50 cps, there was no noticeable effect of frequency on damping energy or compliance. The temperature rise at the interface produced by the mechanical energy dissipated was negligible in the present tests.

The coefficients of friction of 0.70 to 0.83 measured on the crossed cylinder friction rig appear to be characteristic of the oxide layer. For this geometry and normal loading the oxide layer was evidently not removed, so that both the air and vacuum tests were similar. The average coefficient of friction deduced from the gross slip tests in vacuum is close to that of pure aluminum on itself. The coefficient from prolonged gross slip tests in air apparently reflect the mechanical action (e.g., rolling) of wear particles in the interface and the friction coefficient can be even less than that for the solid oxide.

CONCLUSIONS AND RECOMMENDATIONS

Because of the multiplicity of parameters involved in the interface damping phenomena, it is difficult to make any general conclusions. Only a few of the possible parameters were studied in the present tests. However, based upon the present tests with small contact areas, the damping capacity of structures which depend to any extent upon slip at structural interfaces as an energy dissipation mechanism can be decreased when the atmospheric pressure is reduced to a level at which surface oxide layers cannot be maintained. For aluminum, the inability of the surface oxide layer to be maintained in the vacuum environment produced the primary differences between the tests performed in air and vacuum. Aluminum to aluminum surfaces maintain a higher resistance to slip than aluminum oxide to aluminum oxide surfaces and, therefore, more dissipation of mechanical energy occurs in vacuum than air for equal slip displacements. Nearly all metals form oxides of some type; however, the effect of oxide removal will depend upon the relative hardness or friction coefficient between each metal and its oxide. The effect of vacuum on removing other contaminants from surfaces will similarly tend to increase the resistance of joints to slip. It would appear then that for vibration sensitive structures or components exposed to vacuum for any duration, the possibility of significant loss in structural damping should be considered.

Recommendations for future work would include additional studies to determine the relative quantitative importance of the many load, surface, and environmental parameters with respect to energy dissipation in joints.

This would yield insight on how best to control or maintain sufficient damping in a given environment. The studies on small specimens should be extended to simulated structures such as beam, plate, or shell configurations to determine if in these systems the change in damping from air to vacuum environments is predictable. Finally, if structural damping is shown to be harmfully decreased in vacuum, methods for sustaining energy loss mechanisms for structures operating in vacuum should be developed.

REFERENCES

1. H. Shen, S. E. Podlasech, and I. R. Kramer, "Effect of Vacuum on the Fatigue Life of Aluminum," Acta Met., 14, 341, (1966).

2. G. Maidanik, "Energy Dissipation Associated With Gas-Pumping in Structural Joints," J. Acoust. Soc. Am., 40, 1064, (1966); also G. Maidanik and E. E. Ungar, "Panel Loss Factors Due to Gas-Pumping at Structural Joints," NASA CR-954 (1967).

3. T. H. H. Pian and F. C. Hallowell, Jr., "Structural Damping in a Simple Built-up Beam," Proc. 1st U. S. Natl. Cong. of Applied Mechanics, pp. 97-102, June 1951.

4. L. E. Goodman and J. H. Klumpp, "Analysis of Slip Damping With Reference to Turbine-Blade Vibration," J. Appl. Mech., 23, 421, (1956).

5. L. E. Goodman, "A Review of Progress in Analysis of Interfacial Slip Damping," Structural Damping, J. Ruzika, Ed., ASME, New York, 1959.

6. N. G. Kalinen, Yu. A. Lebedev, et al., "Structural Damping in Permanent Joints," WP-AFB, Ohio, FTD-TT-63-755/1+2, 191 pages, (1963).

7. E. E. Ungar, "Energy Dissipation at Structural Joints; Mechanics and Magnitudes," WP-AFB, Ohio, FDL-TDR-64-98, August 1964.

8. R. R. McWithey and R. J. Hayduk, "Damping Characteristics of Built-up Cantilever Beams in a Vacuum Environment," NASA TN D-3065, Nov. 1965.

9. R. D. Mindlin, "Compliance of Elastic Bodies in Contact," J. Appl. Mech., 16, 259, (1949).

10. R. D. Mindlin, W. P. Mason, T. F. Osmer, and H. Deresiewicz, "Effects of an Oscillating Tangential Force on the Contact Surfaces of Elastic Spheres," Proc. 1st U. S. Natl. Cong. of Applied Mechanics, ASME, pp. 203-208, (1952).

11. L. E. Goodman and C. B. Brown, "Energy Dissipation in Contact Friction: Constant Normal and Cyclic Tangential Loading," J. Appl. Mech., 29, 17, (1962).

12. R. V. Klint, "Oscillating Tangential Forces on Cylindrical Specimens in Contact at Displacements Within the Region of No Gross Slip," ASLE Preprint No. 60 AM 6C5, (1960).

13. F. P. Bowden and D. Tabor, The Friction and Lubrication of Solids, Oxford University Press, 1954.

14. R. D. Brown and R. A. Burton, "Friction and Adhesion of Copper in Vacuum," Jour. of Lub. Tech., 1, (1967).

15. D. H. Buckley, M. Swikert, and R. L. Johnson, "Friction, Wear, and Evaporation Rates of Materials in Vacuum to 10^{-7} mmHg," ASLE Trans., 5, (1962).

16. R. D. Brown, R. A. Burton, and P. M. Ku, "Long-Duration Lubrication Studies in Simulated Space Vacuum," ASLE Trans., 7, 3, (1964).

17. S. Dushman, Scientific Foundations of Vacuum Technique, 2nd Ed., John Wiley and Sons, New York, p. 87, (1962).

18. R. W. Wilson, "The Contact Resistance and Mechanical Properties of Surface Films on Metals," Proc. Phys. Soc., 68, 9-B, 625 (1955).

19. J. R. Whitehead, "Surface Deformation and Friction of Metals at Light Loads," Proc. Roy. Soc., 22, 109, (1951).

20. G. W. Cunningham and J. W. Spretnak, "A Study of the Effect of Applied Pressure on Surface Contact Area," Int. Jour. Mechanical Sciences, 4, 231, (1964).

21. P. E. D'yachenko, N. N. Tolkacheva, G. A. Andrew, and T. M. Karpova, "The Actual Contact Area Between Touching Surfaces," Consultants Bureau, New York, 1964.

22. T. Tsukizoe and T. Hisakado, "On the Mechanism of Contact Between Metal Surfaces--The Penetrating Depth and the Average Clearance," ASME Paper No. 64-Lub-18, (1964).

23. J. A. Greenwood and J. B. P. Williamson, "The Contact of Rough Surfaces," Part I, Burndy Corporation Research Report.

24. A. F. Metherell and S. V. Diller, "Instantaneous Energy Dissipation Rate in a Lap Joint--Uniform Clamping Pressure," J. Appl. Mech., 35, 123, (1968).

25. Metals Handbook, 8th Ed., 1, American Society for Metals, 1961.

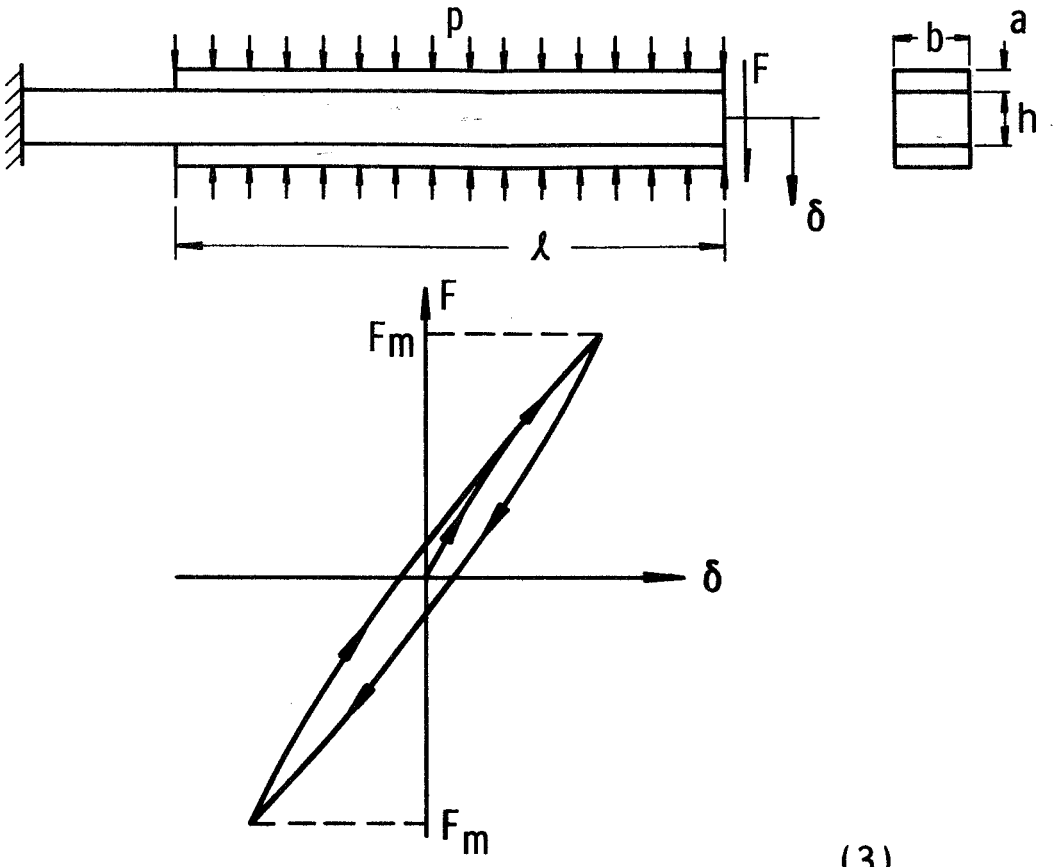

Figure 1a. Cantilever Beam Of Pian And Hallowell [3]

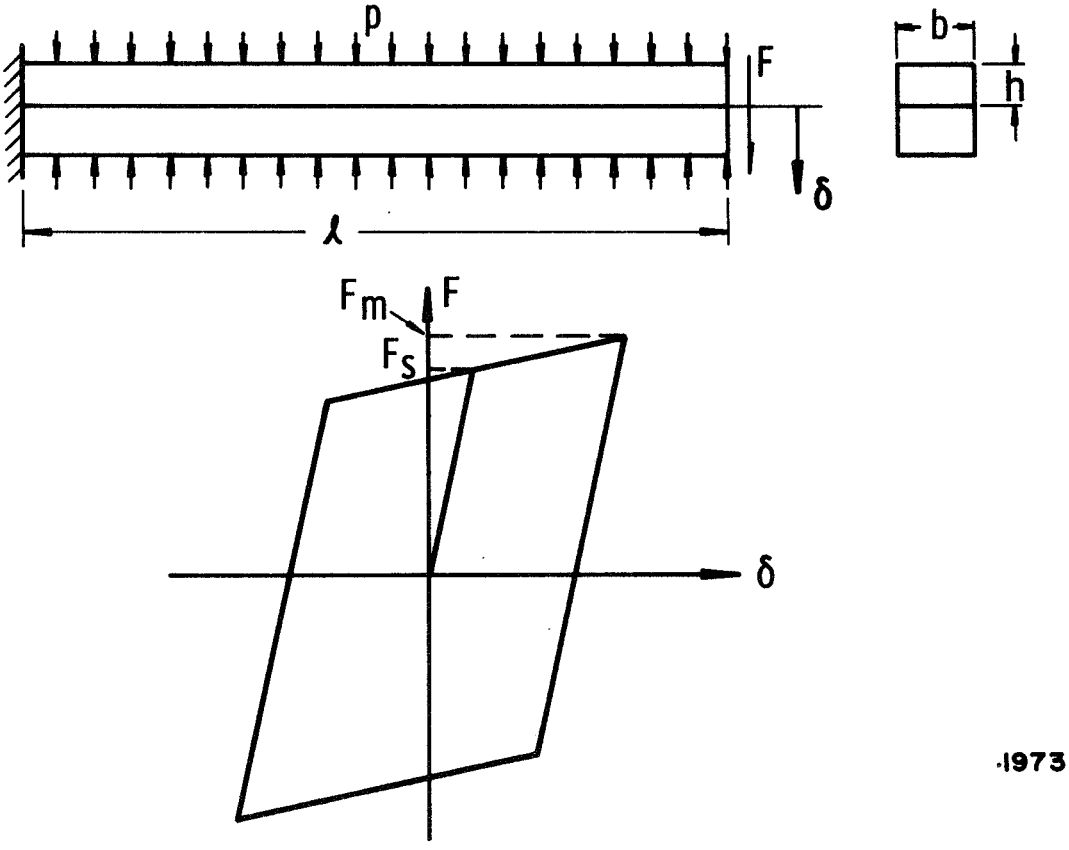

1973

Figure 1b. Cantilever Beam Of Goodman And Klumpp [4]

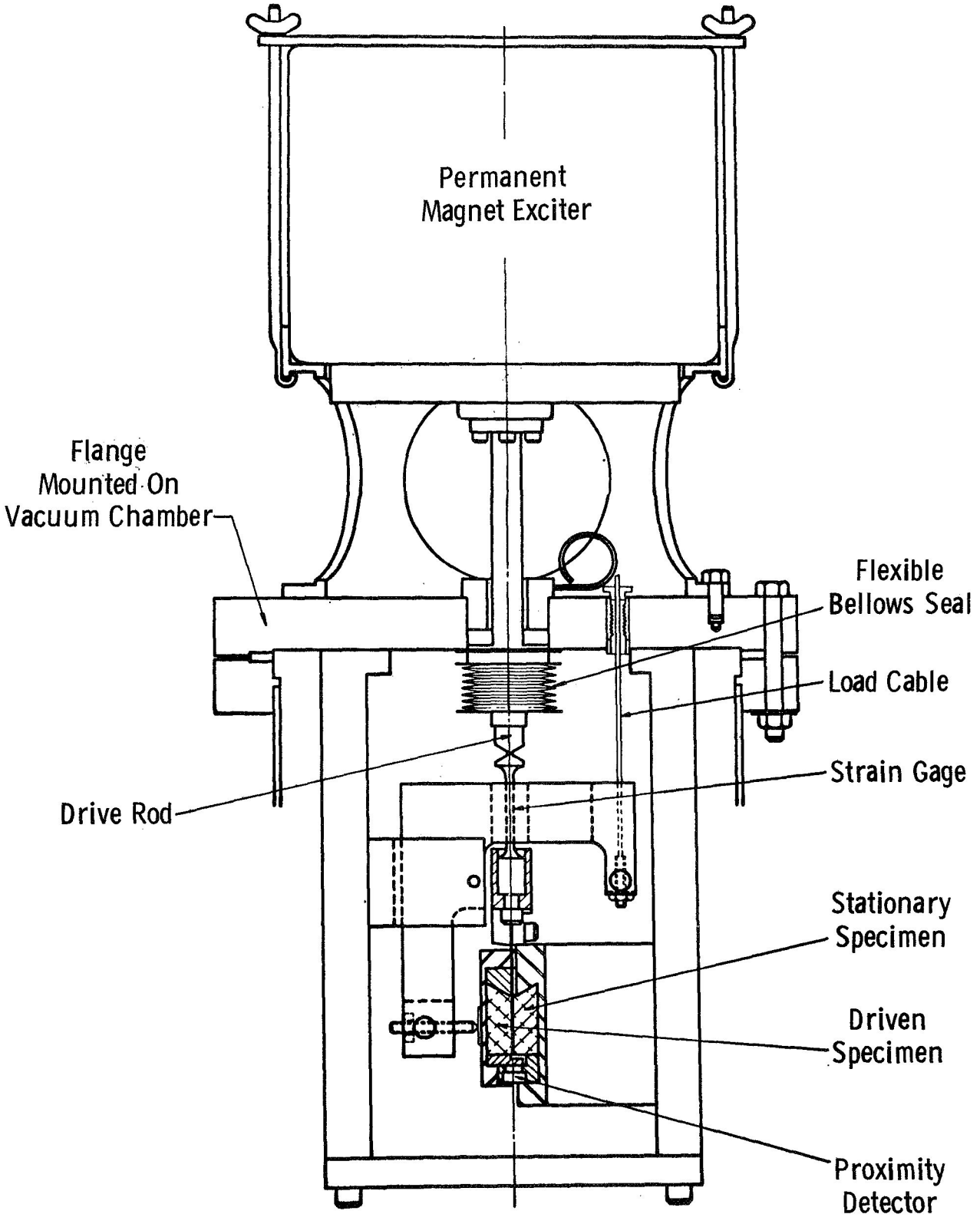

Figure 2a. Interface Damping Apparatus

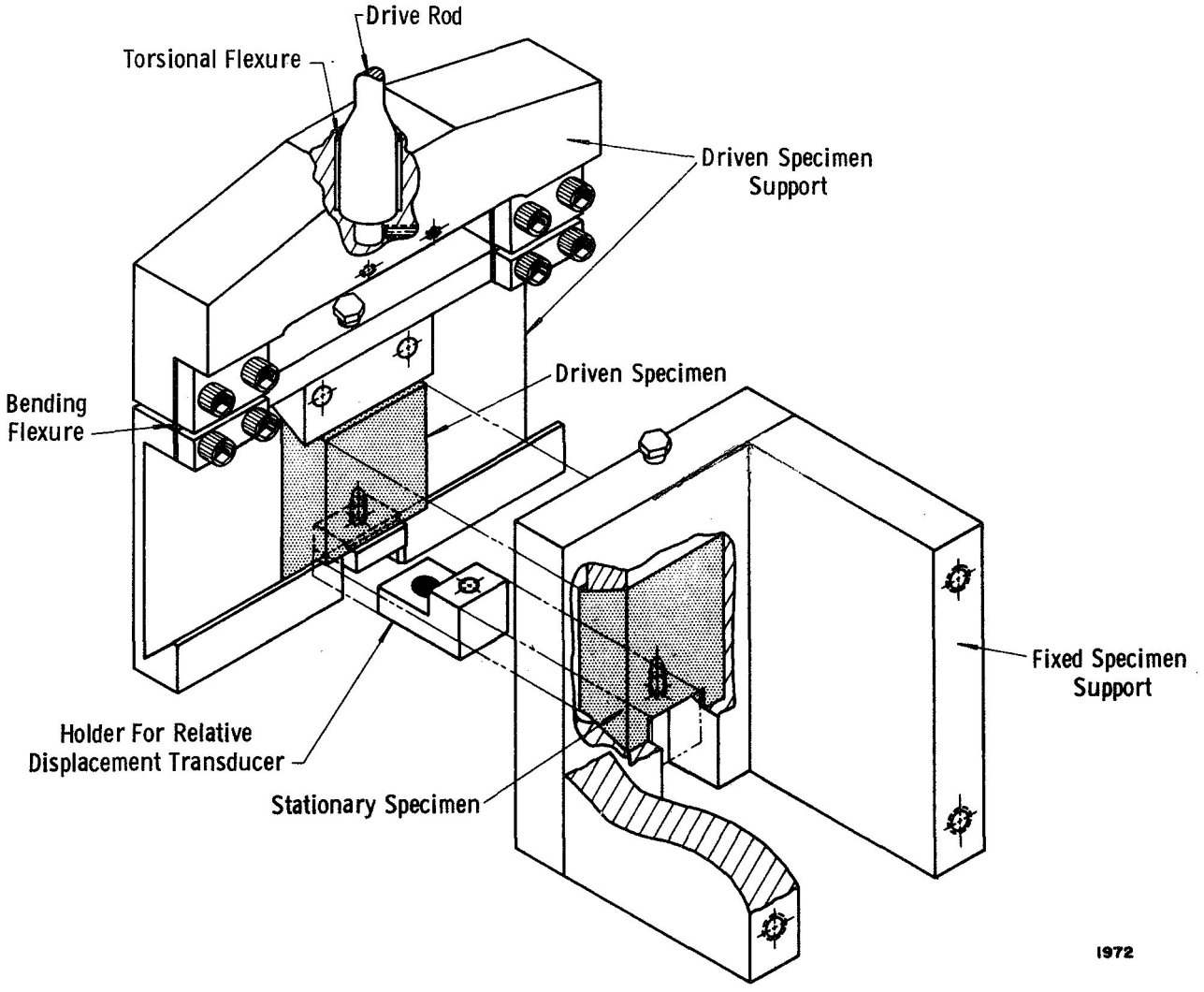

Figure 2b. Details Of Specimen Holder

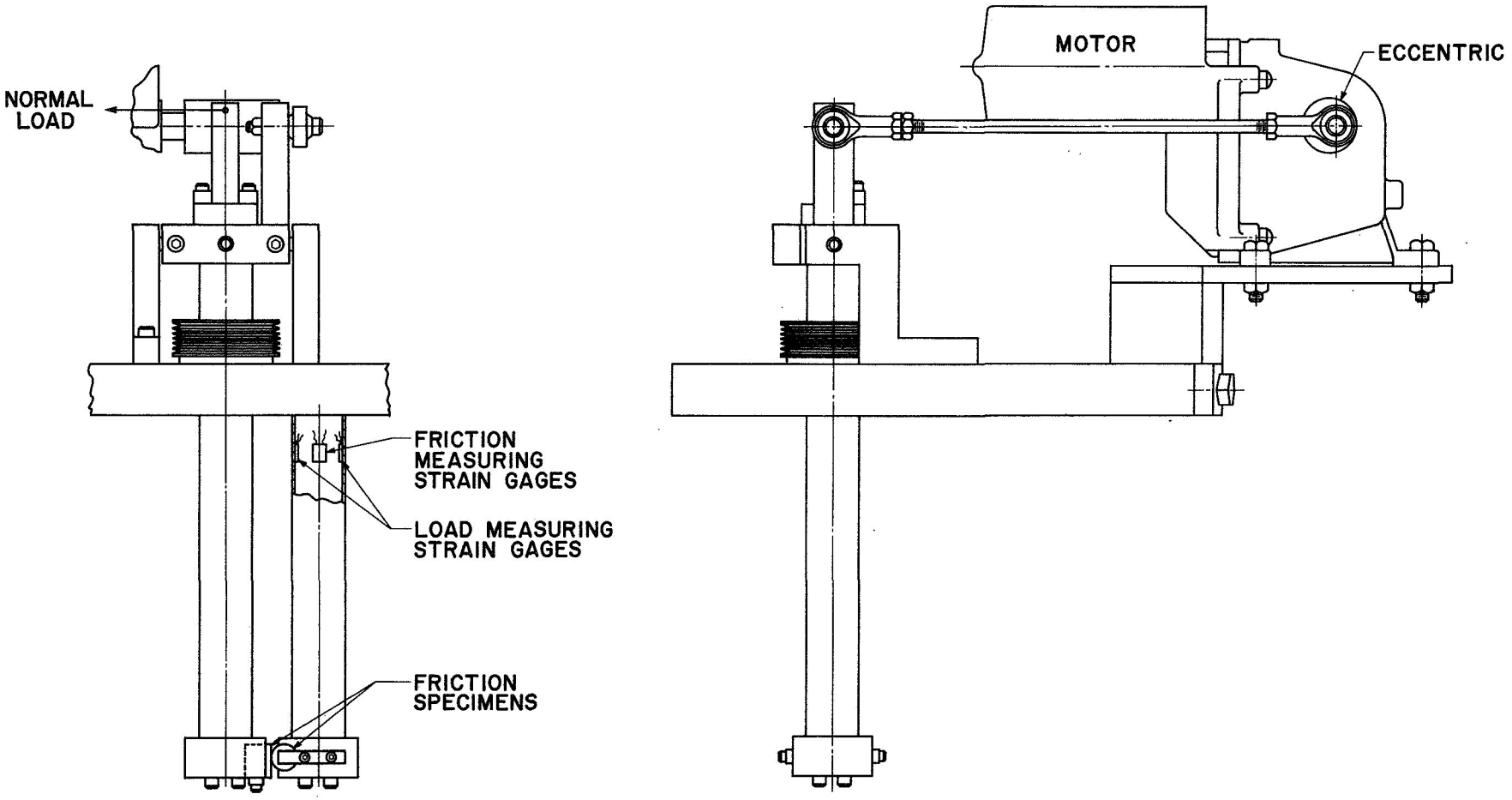

FIGURE 3. ASSEMBLY OF OSCILLATING FRICTION APPARATUS

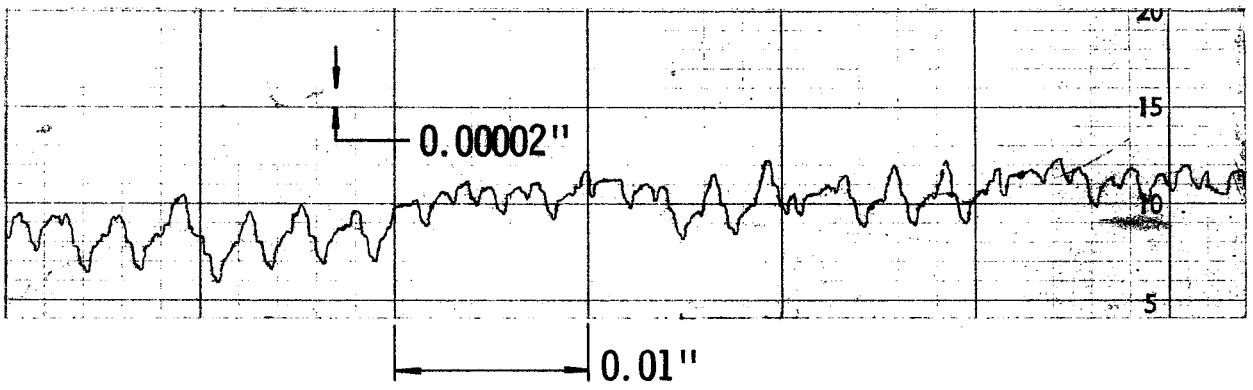

Figure 4a. Typical Surface Profile At 90° To Flycut Ridges

Figure 4b. Orientation Of Ridges On Mating Specimens

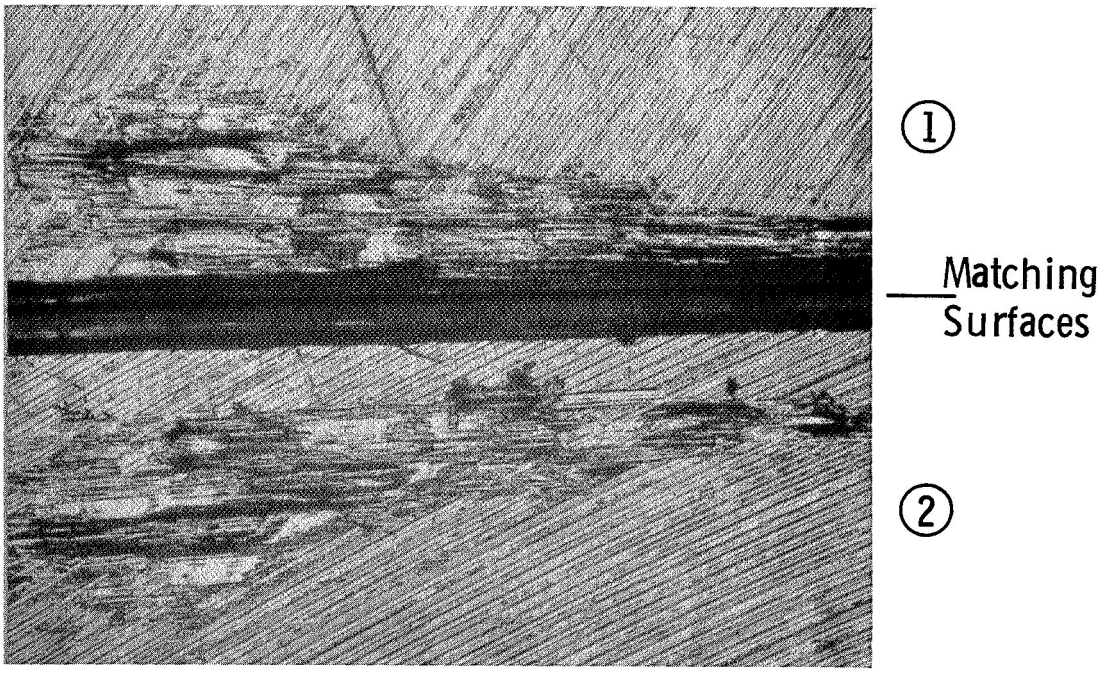

After Gross Slip In Vacuum

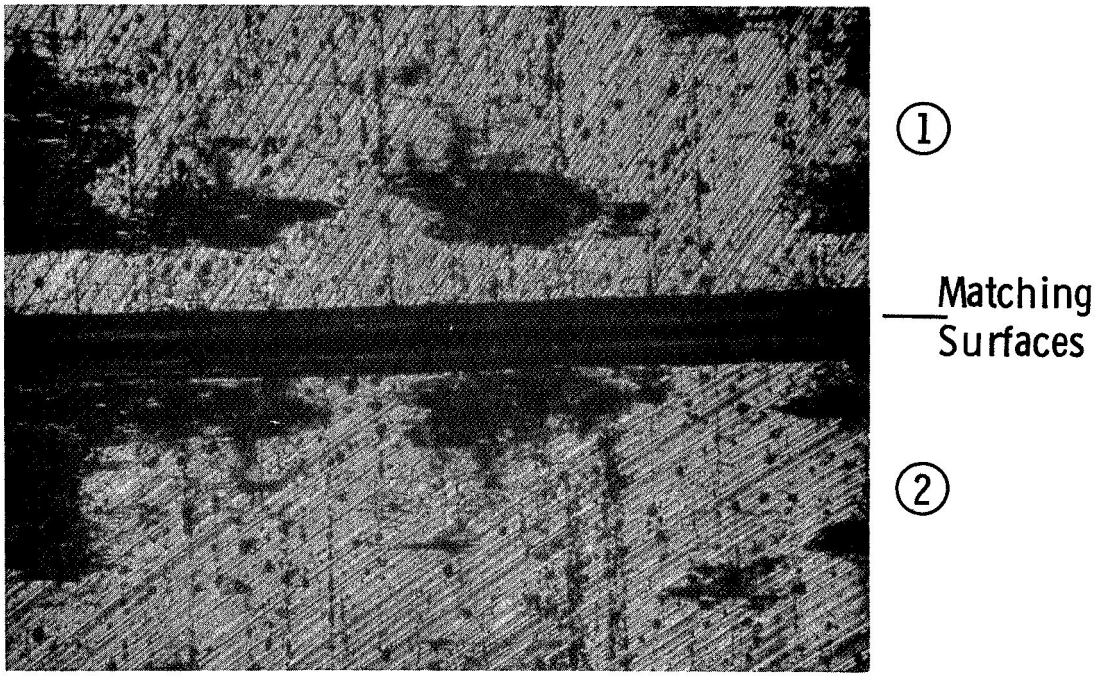

After Gross Slip In Air

Figure 5. Effect Of Atmosphere On Gross Slip Surface Damage

60 X

Figure 6. Typical Wear Debris Resulting From Gross Slip In Air

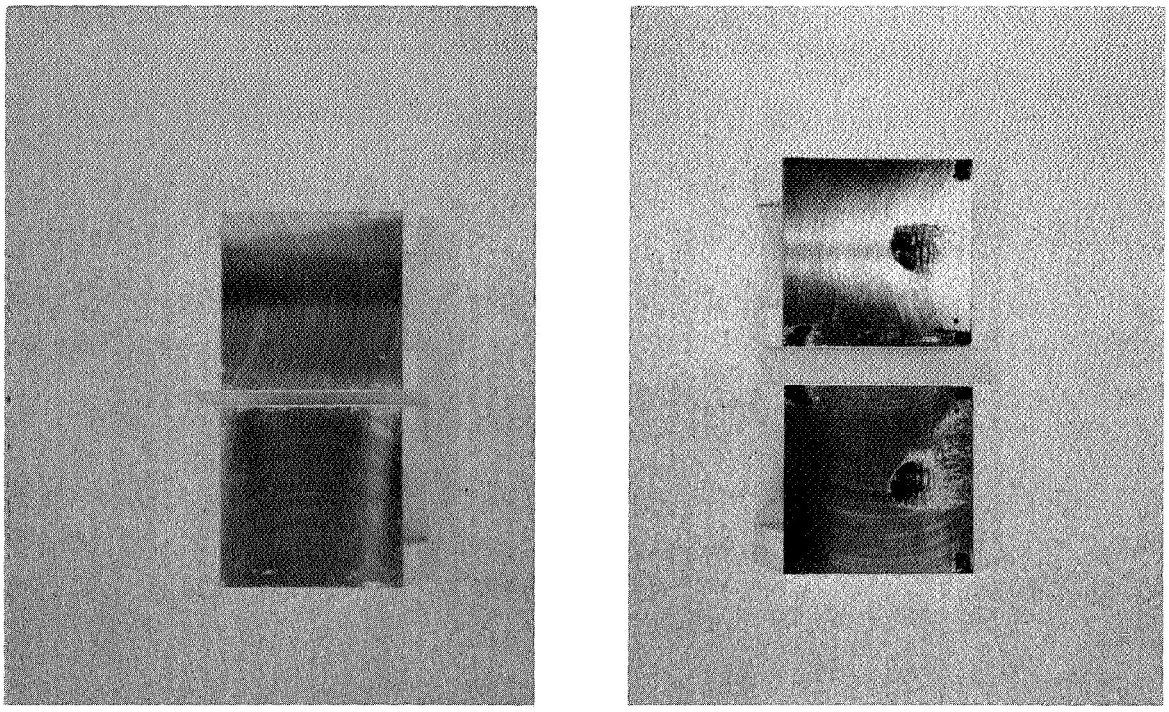

After Gross Slip
In Vacuum

After Gross Slip
In Air

Figure 7. Distribution Of Contact Areas On Flycut Specimens After Gross Slip

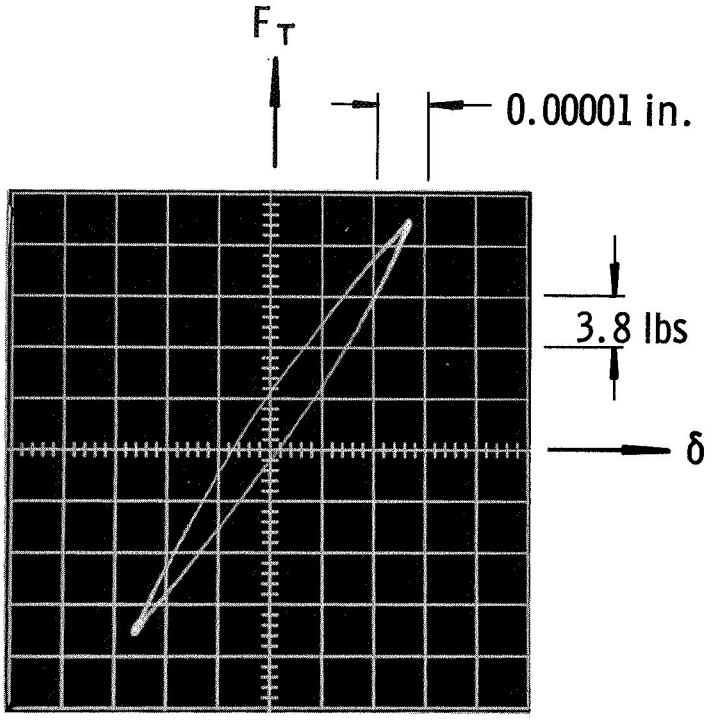

Figure 8. Typical Microslip Hysteresis Loop

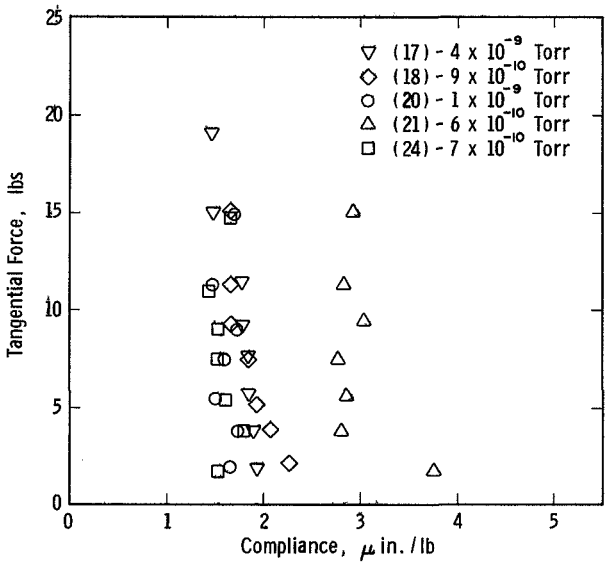

Figure 9. Compliance During Initial Runs In Vacuum

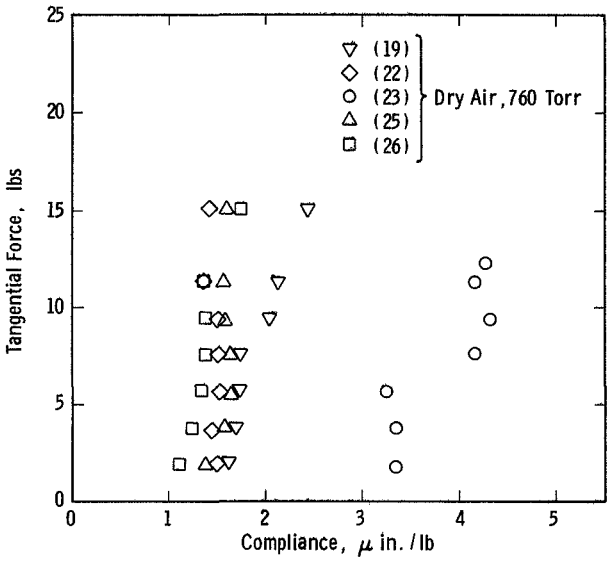

Figure 10. Compliance During Initial Runs In Air

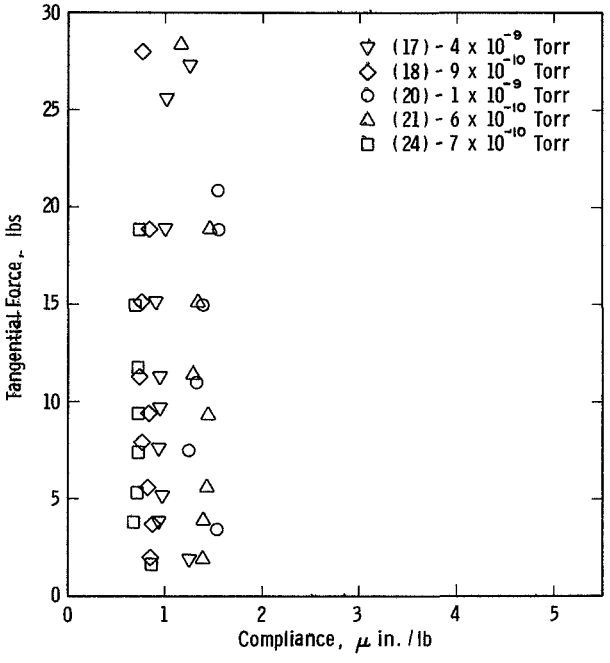

Figure 11. Compliance After Extensive Gross Slip In Vacuum

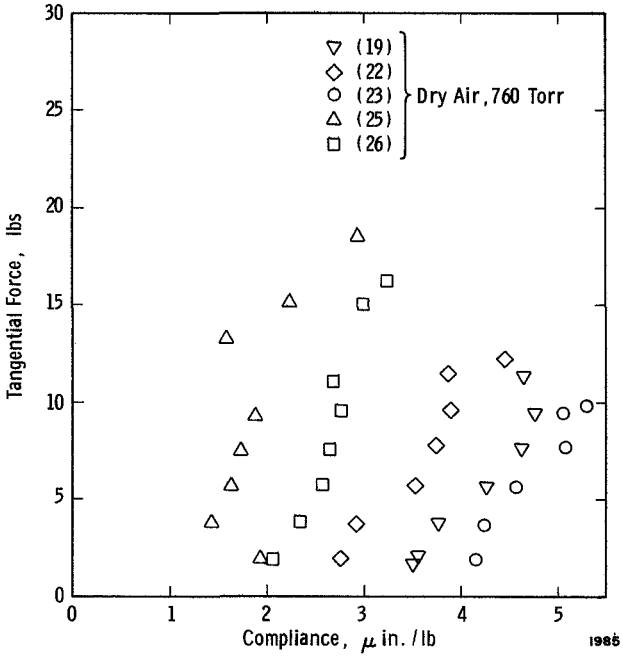

Figure 12. Compliance After Extensive Gross Slip In Air

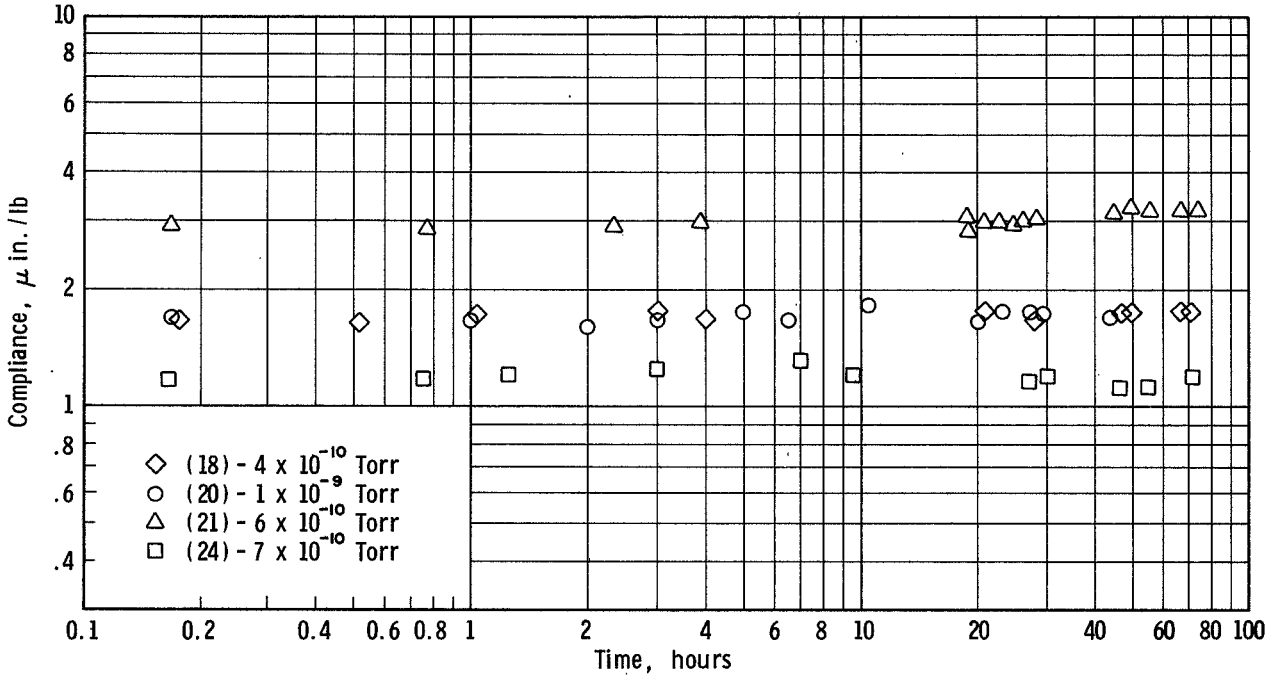

Figure 13. Compliance Versus Time For Runs In Vacuum

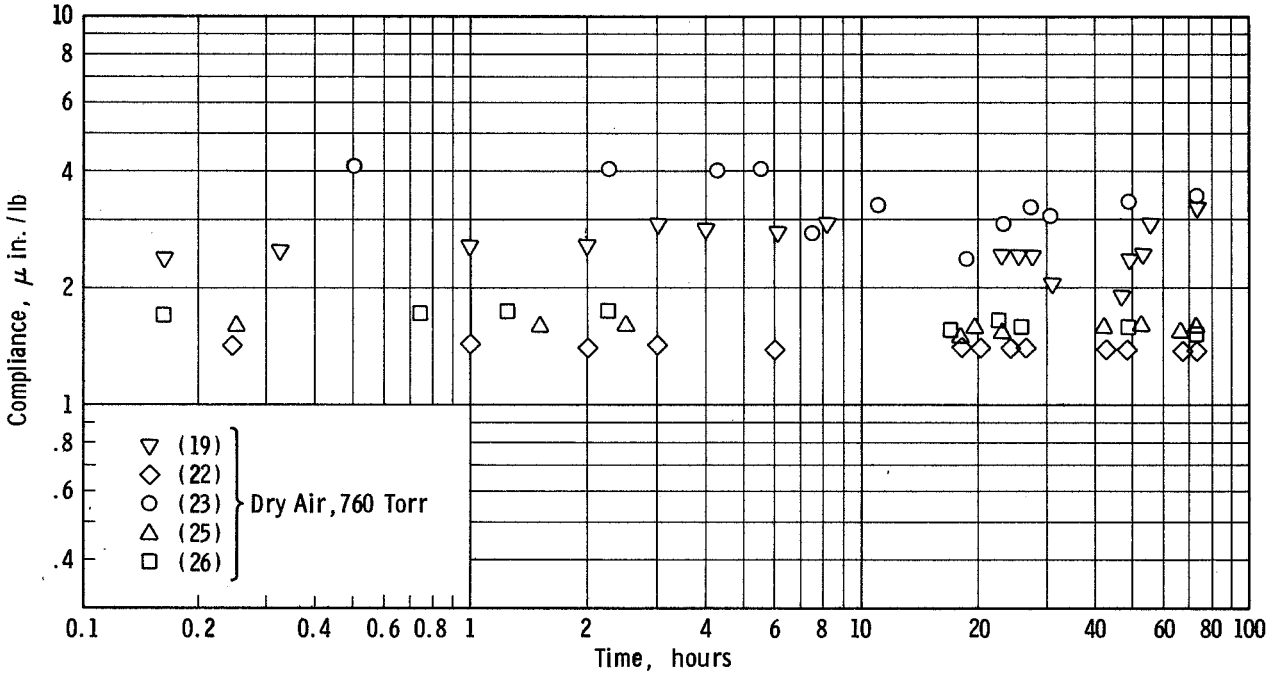

Figure 14. Compliance Versus Time For Runs In Air

1974

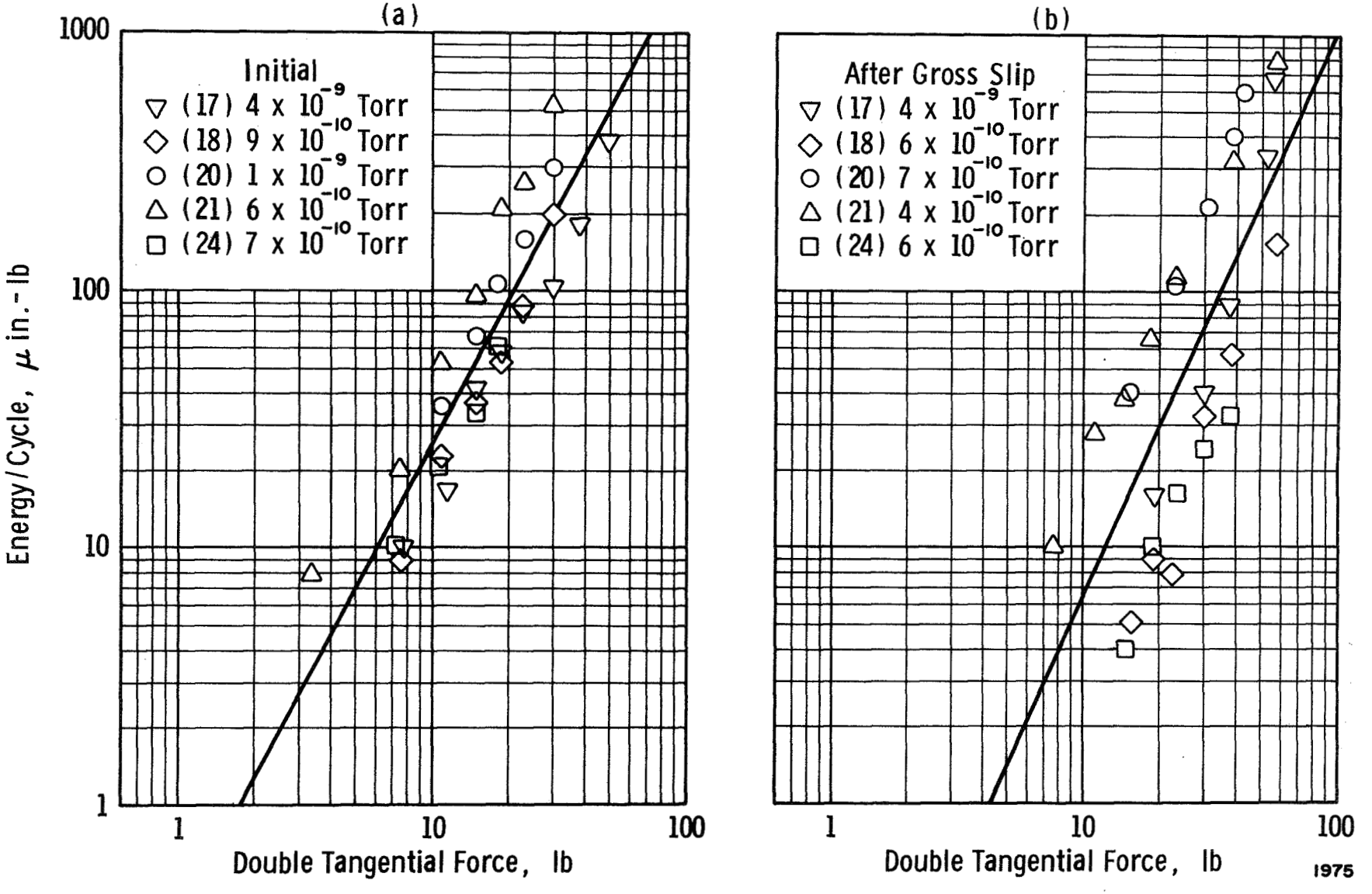

Figure 15. Energy Dissipation Per Cycle vs Tangential Force Before And After Gross Slip In Vacuum

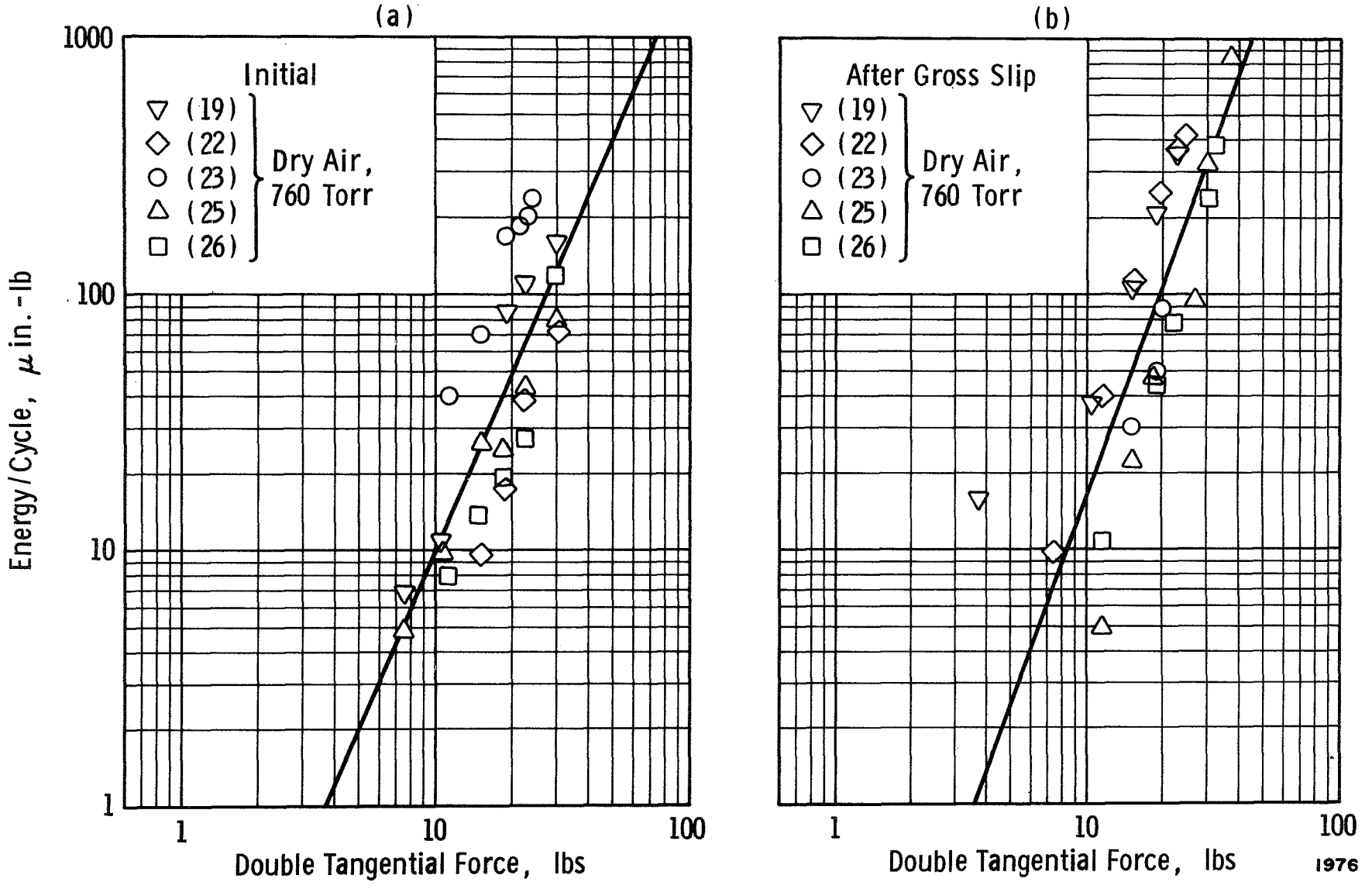

Figure 16. Energy Dissipation Per Cycle vs Tangential Force Before And After Gross Slip In Air

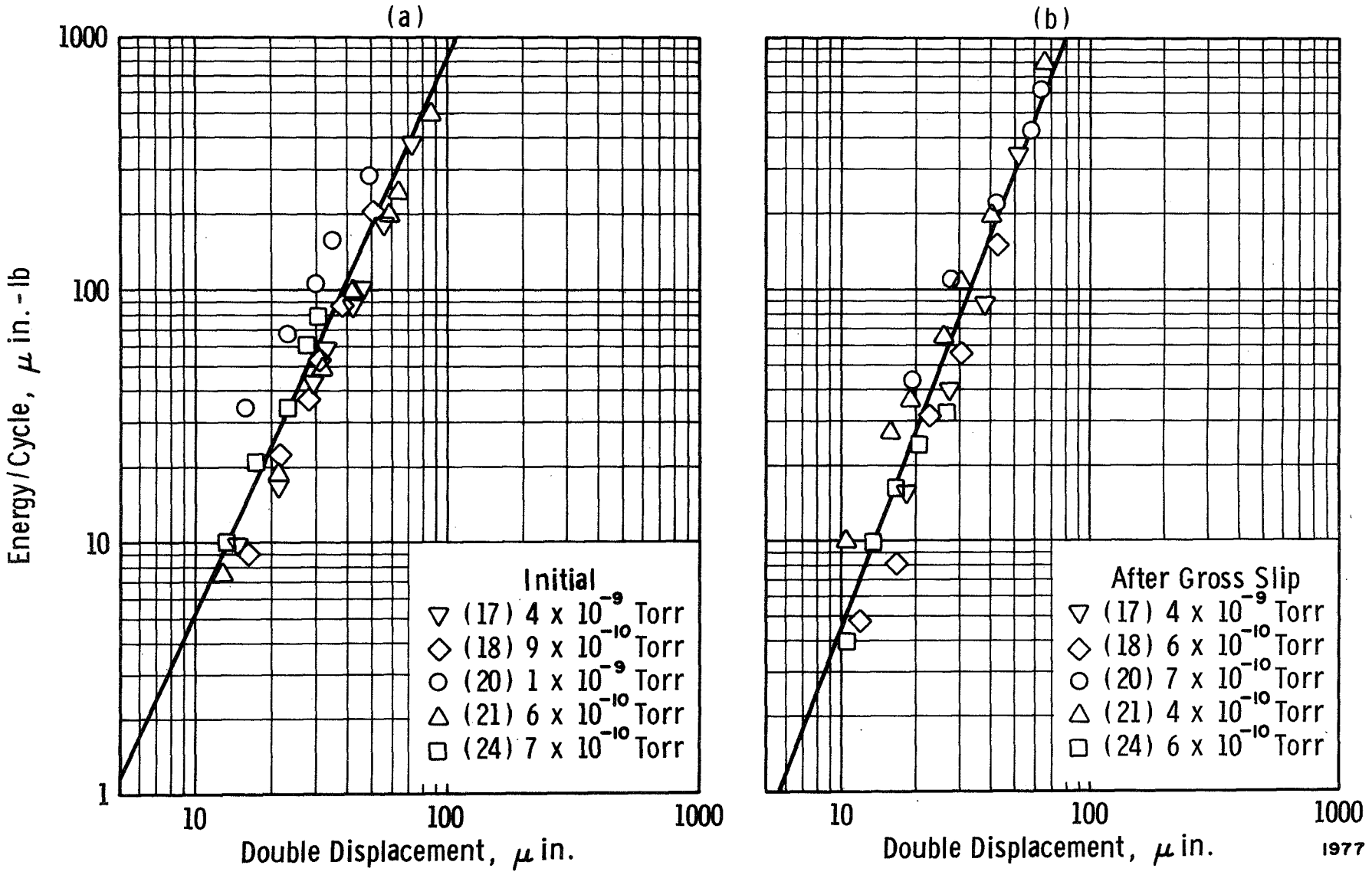

Figure 17. Energy Dissipation Per Cycle vs Displacement Before And After Gross Slip In Vacuum

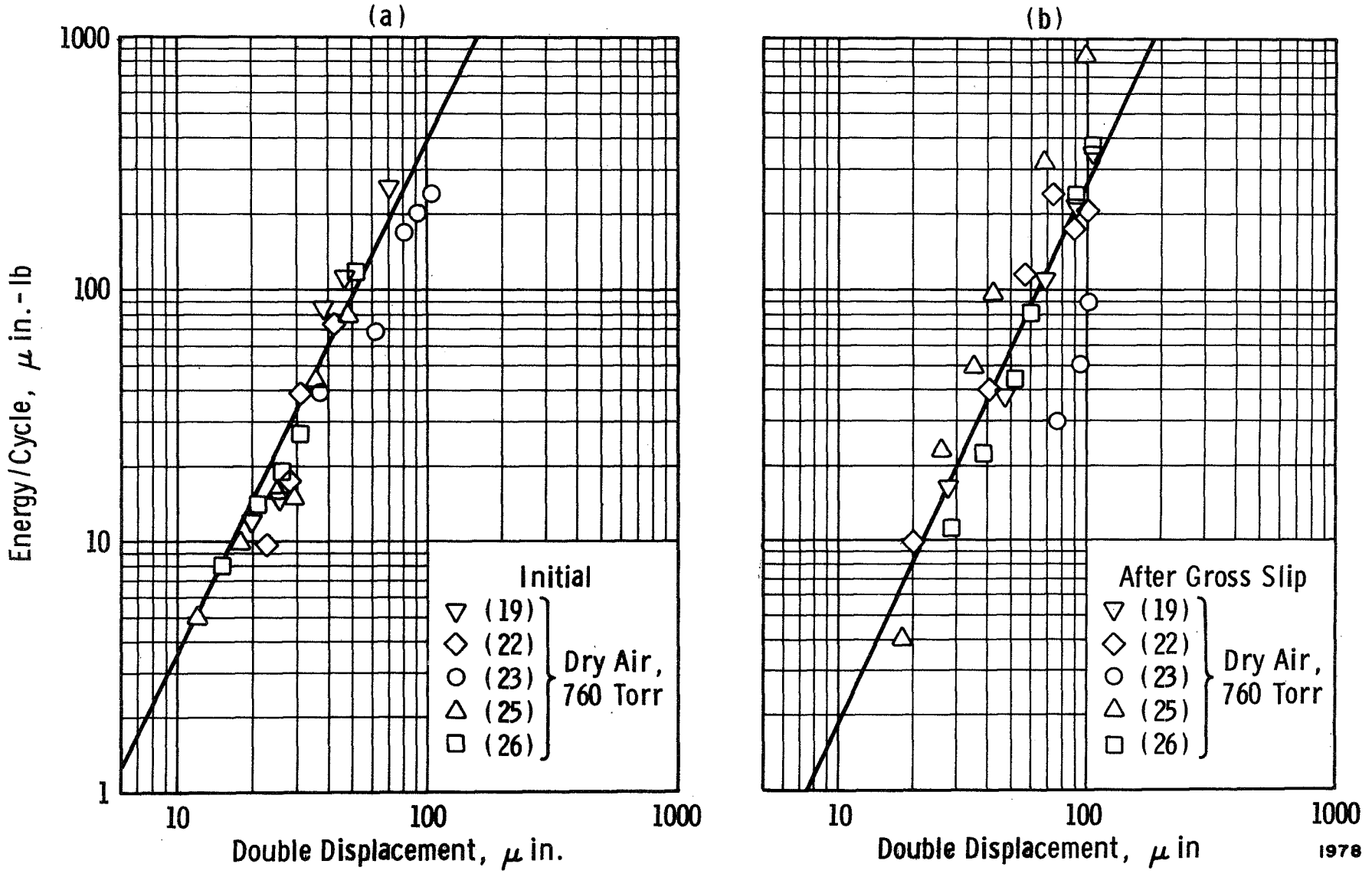

Figure 18. Energy Dissipation Per Cycle vs Displacement Before And After Gross Slip In Air

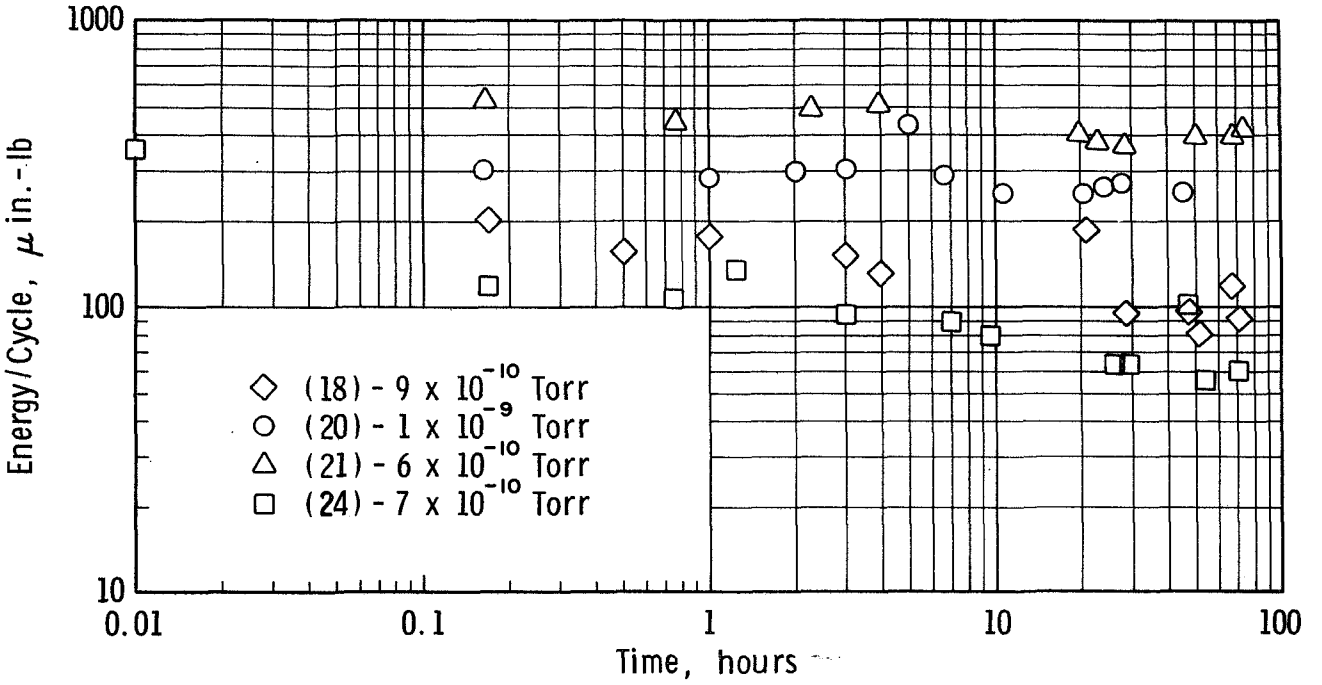

Figure 19. Energy Versus Time During Long-Duration Microslip Oscillation In Vacuum

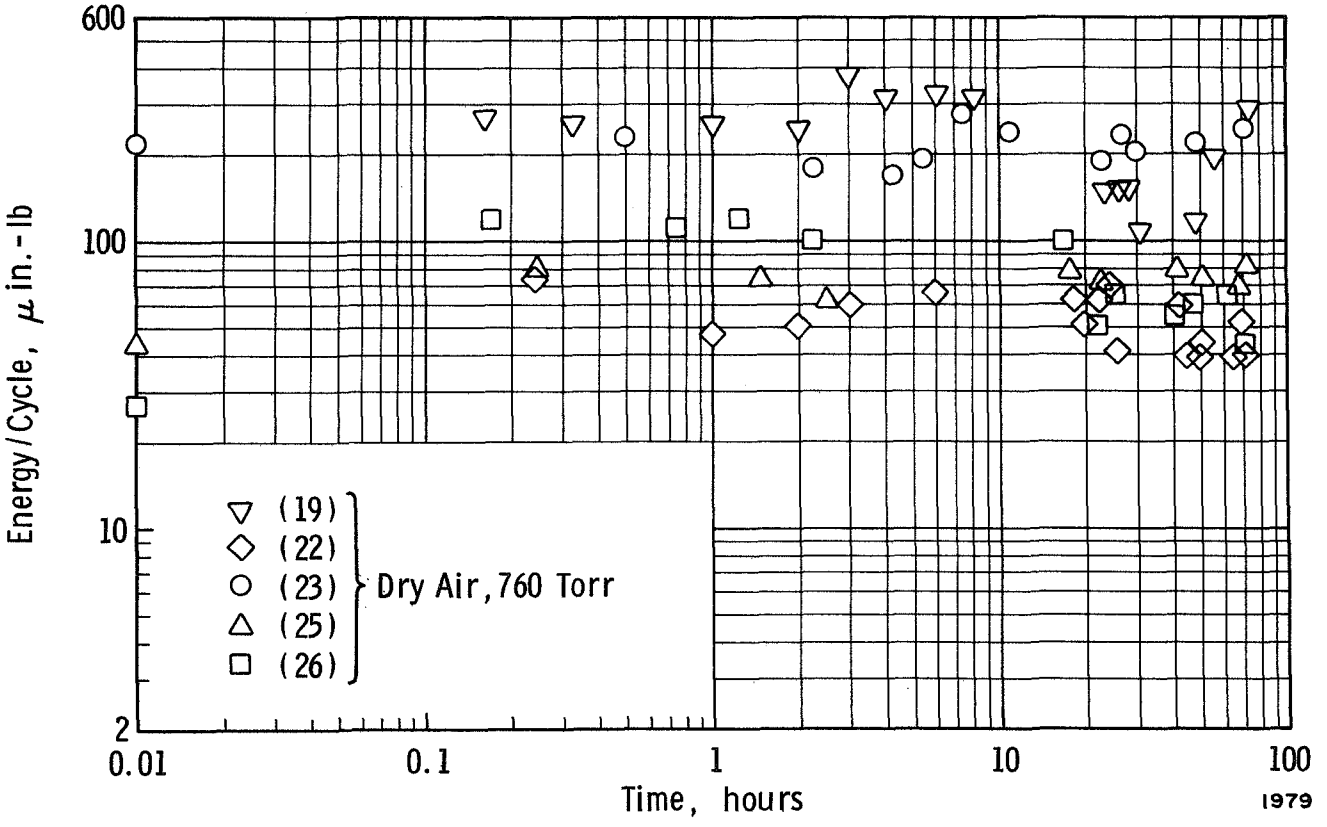

Figure 20. Energy Versus Time During Long-Duration Microslip Oscillation In Air

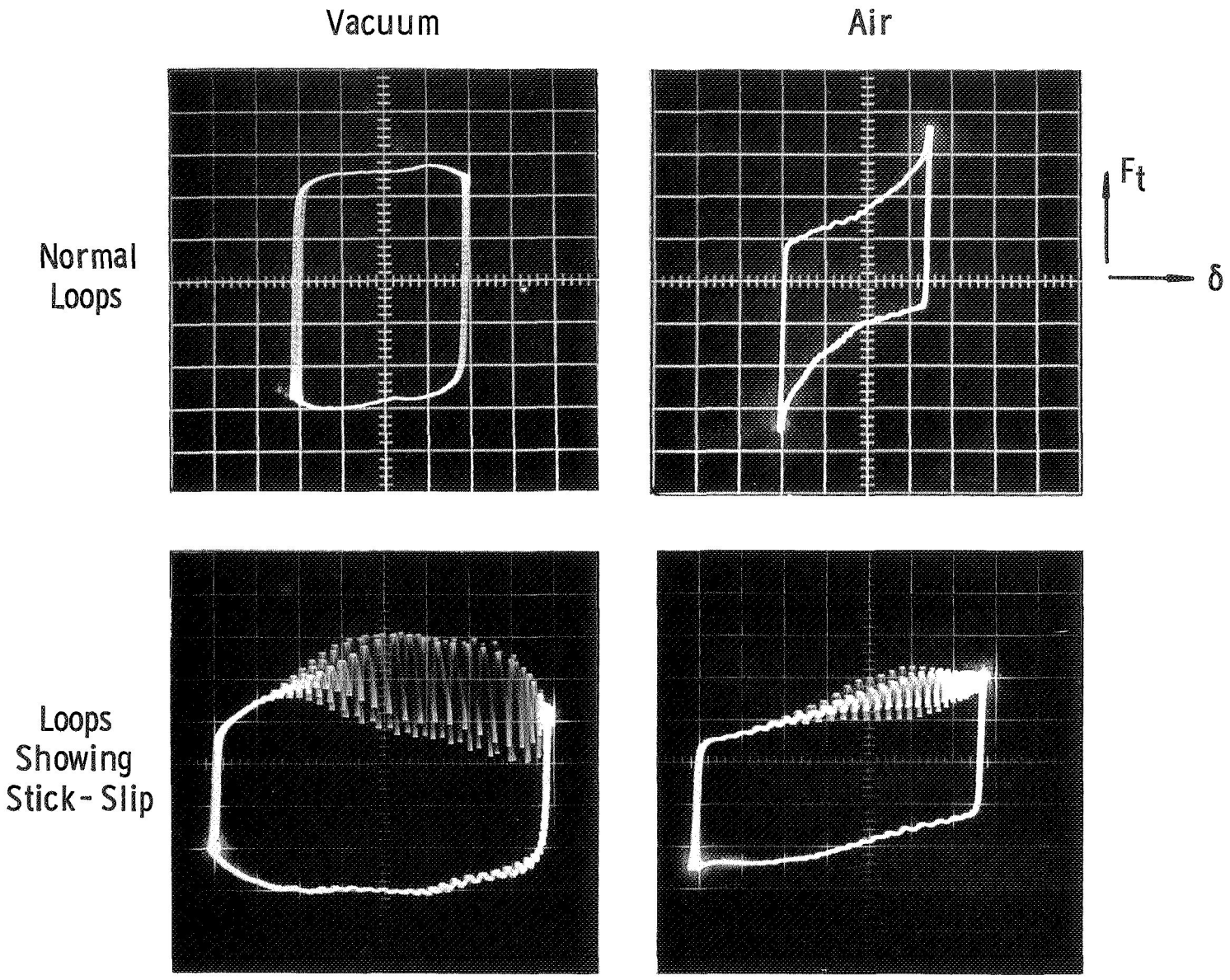

Figure 21. Typical Gross Slip Hysteresis Loops
($F_t \simeq 3.8$ lbs/cm, $\delta \simeq 500$ microinch/cm)

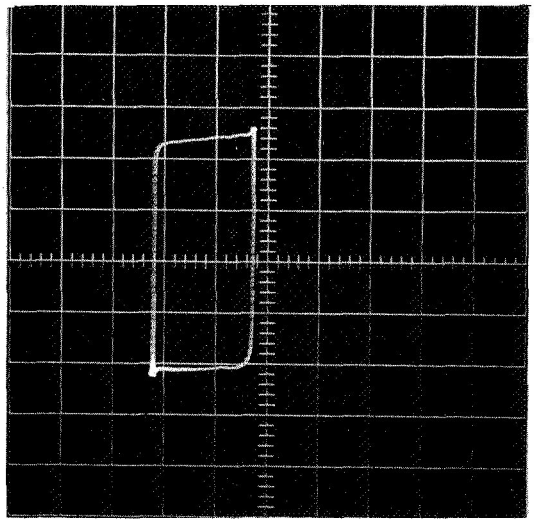

After 30 seconds

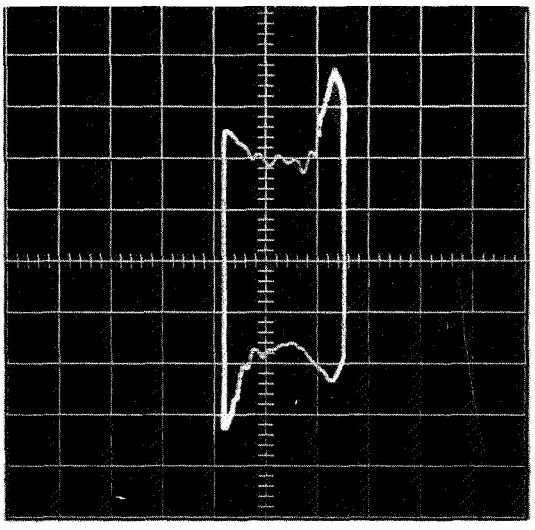

After 1 hour

Figure 22. Gross Slip Hysteresis Loops For Specimens In Nitrogen At 760 Torr

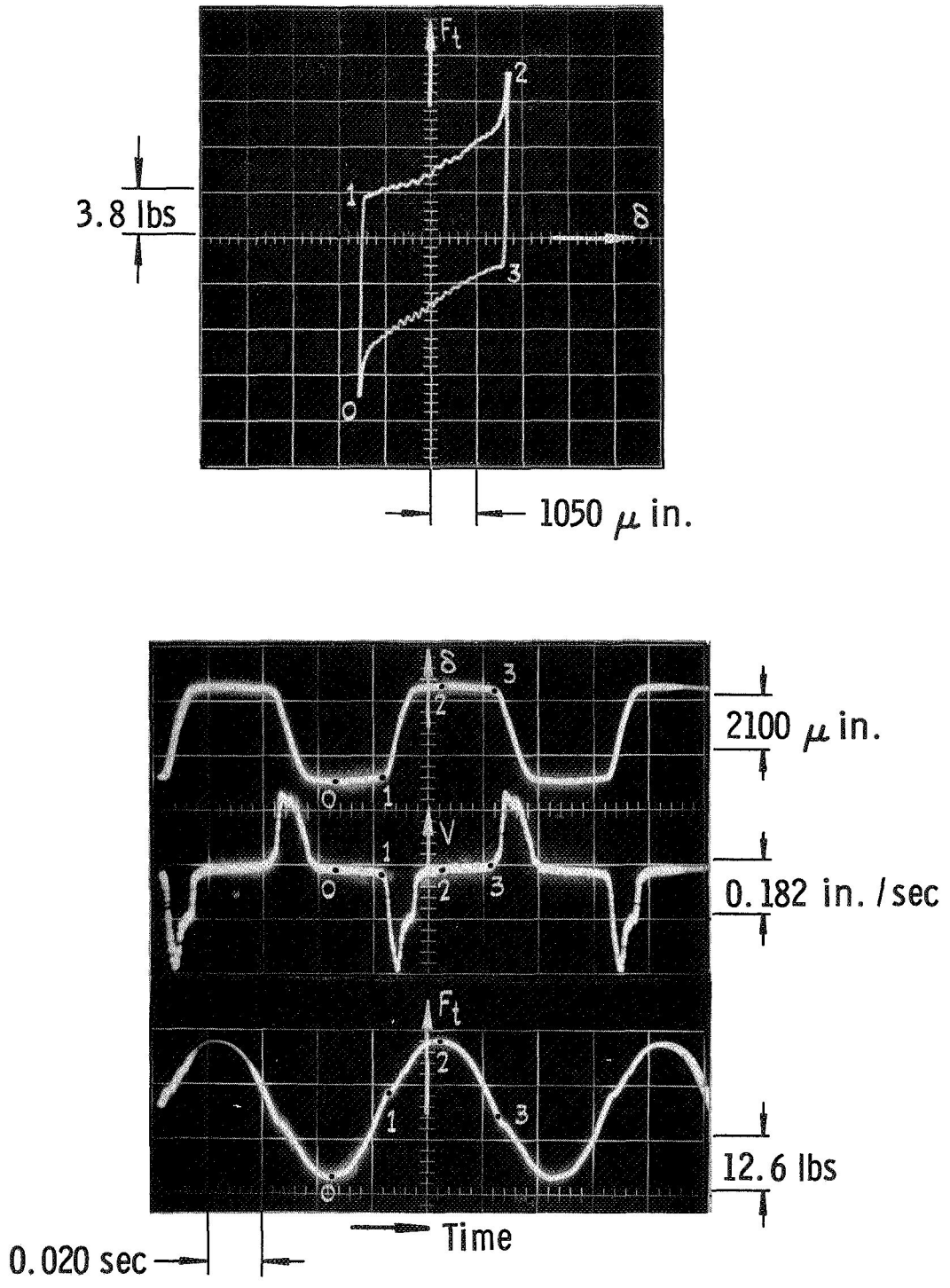

Figure 23. Hysteresis Loop And Corresponding Time Traces Of Displacement Velocity And Force During Gross Slip Oscillation In Air

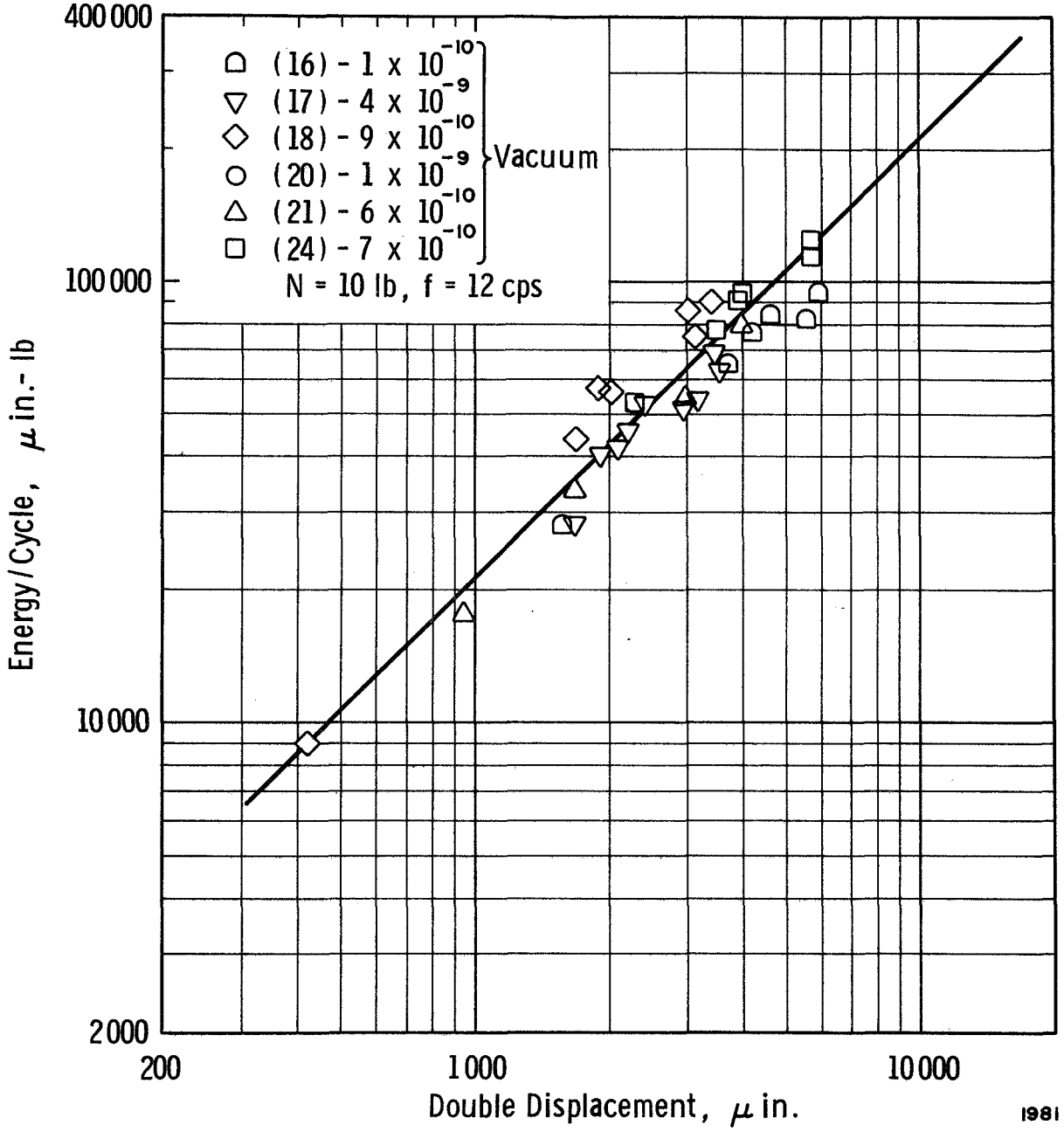

Figure 24. Energy vs Displacement During Gross Slip Oscillation In Vacuum

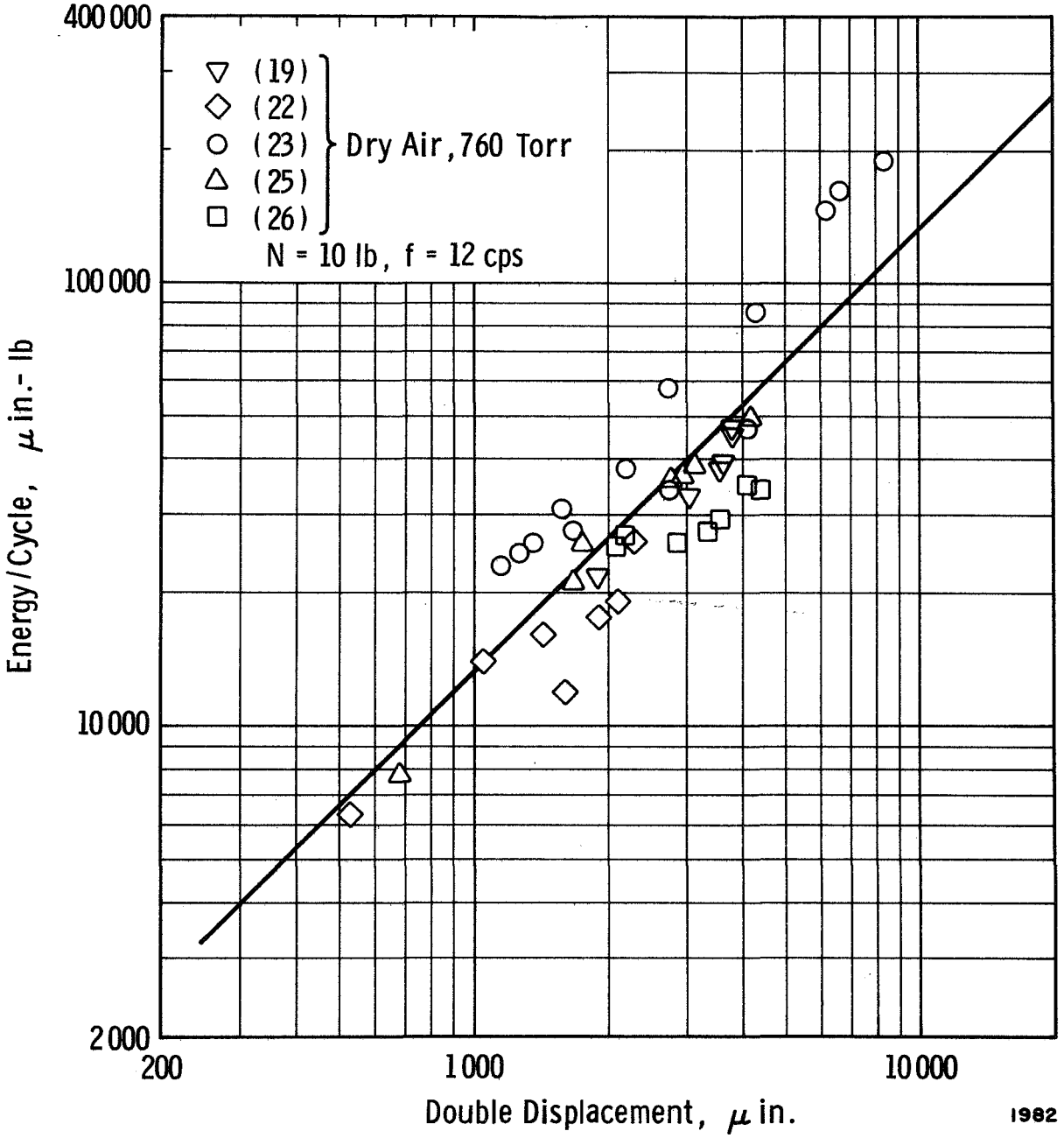

Figure 25. Energy vs Displacement During Gross Slip Oscillation In Air

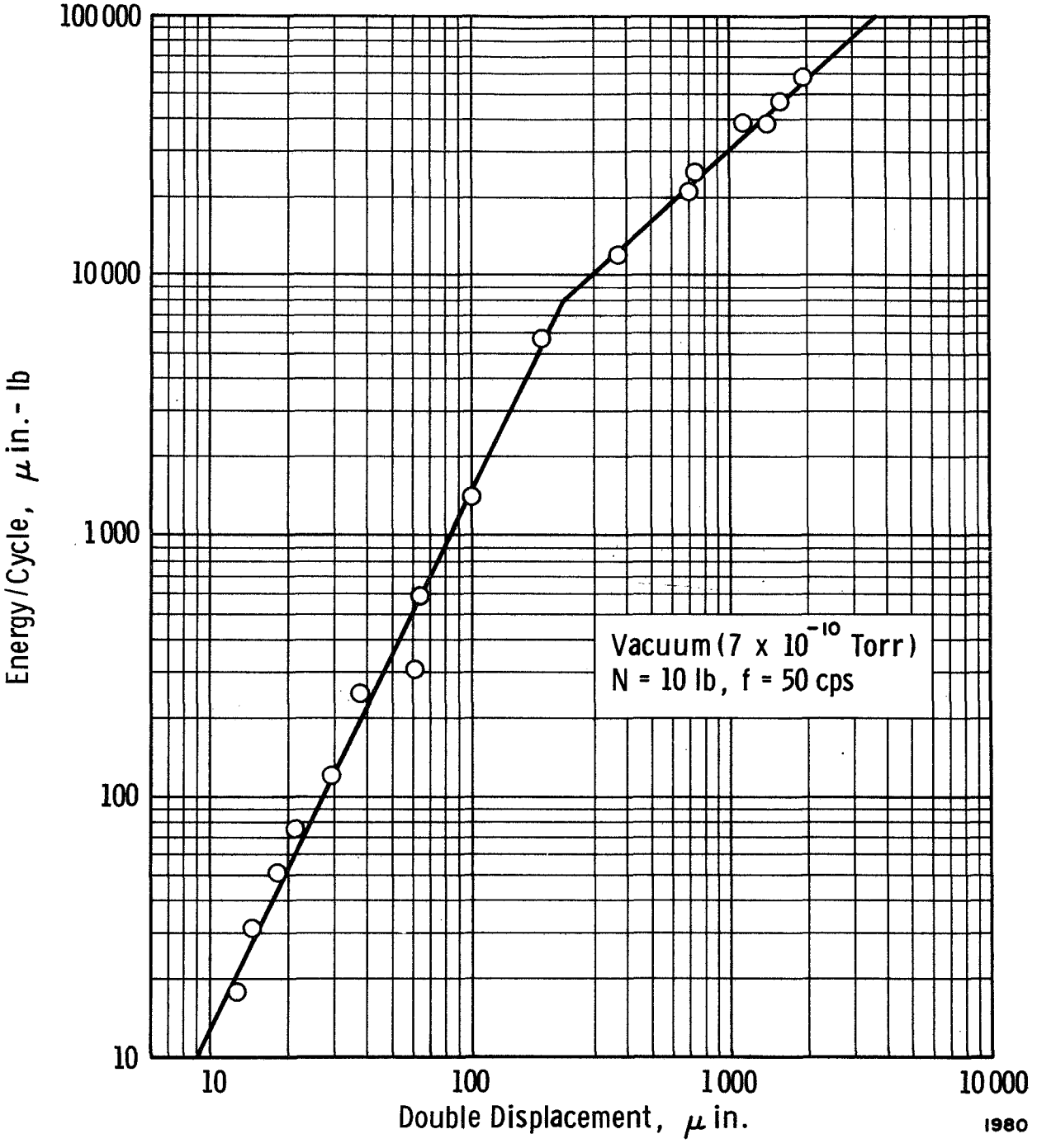

Figure 26. Energy vs Displacement During Microslip And Gross Slip Oscillation

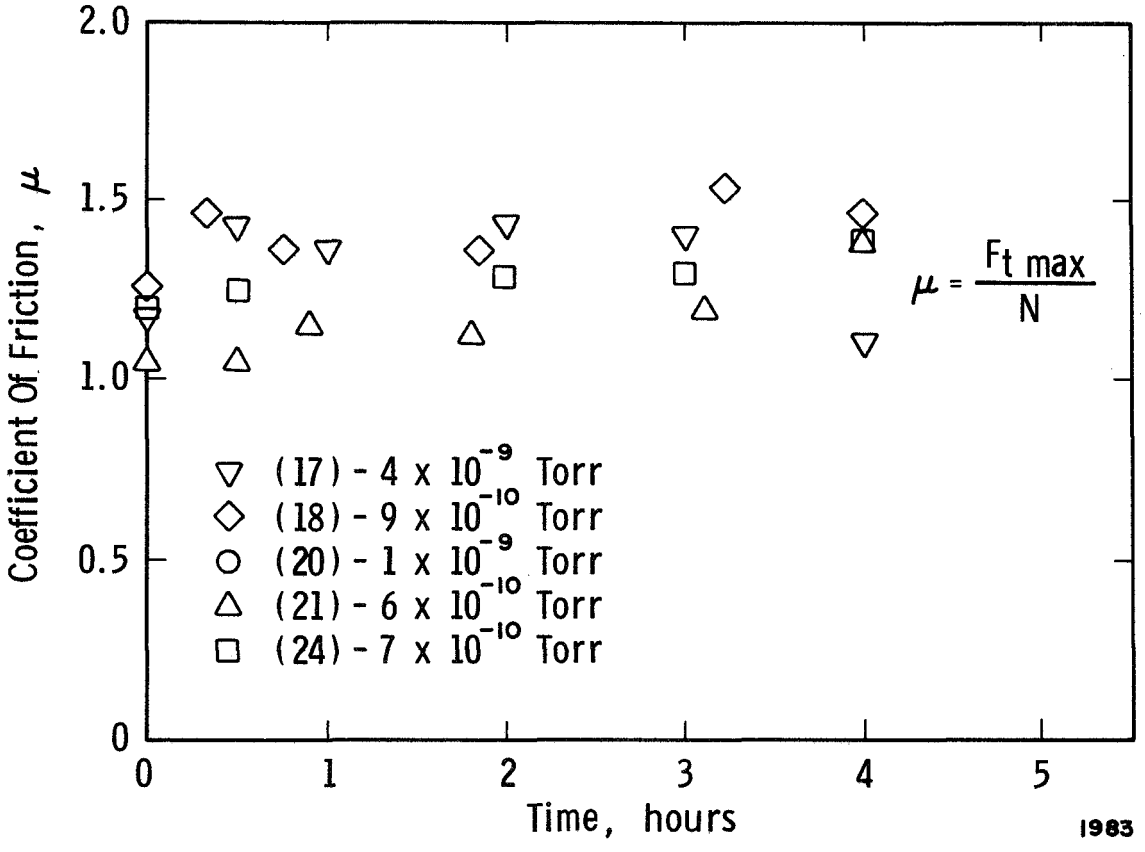

Figure 27. Coefficient Of Friction During Gross Slip Oscillation In Vacuum

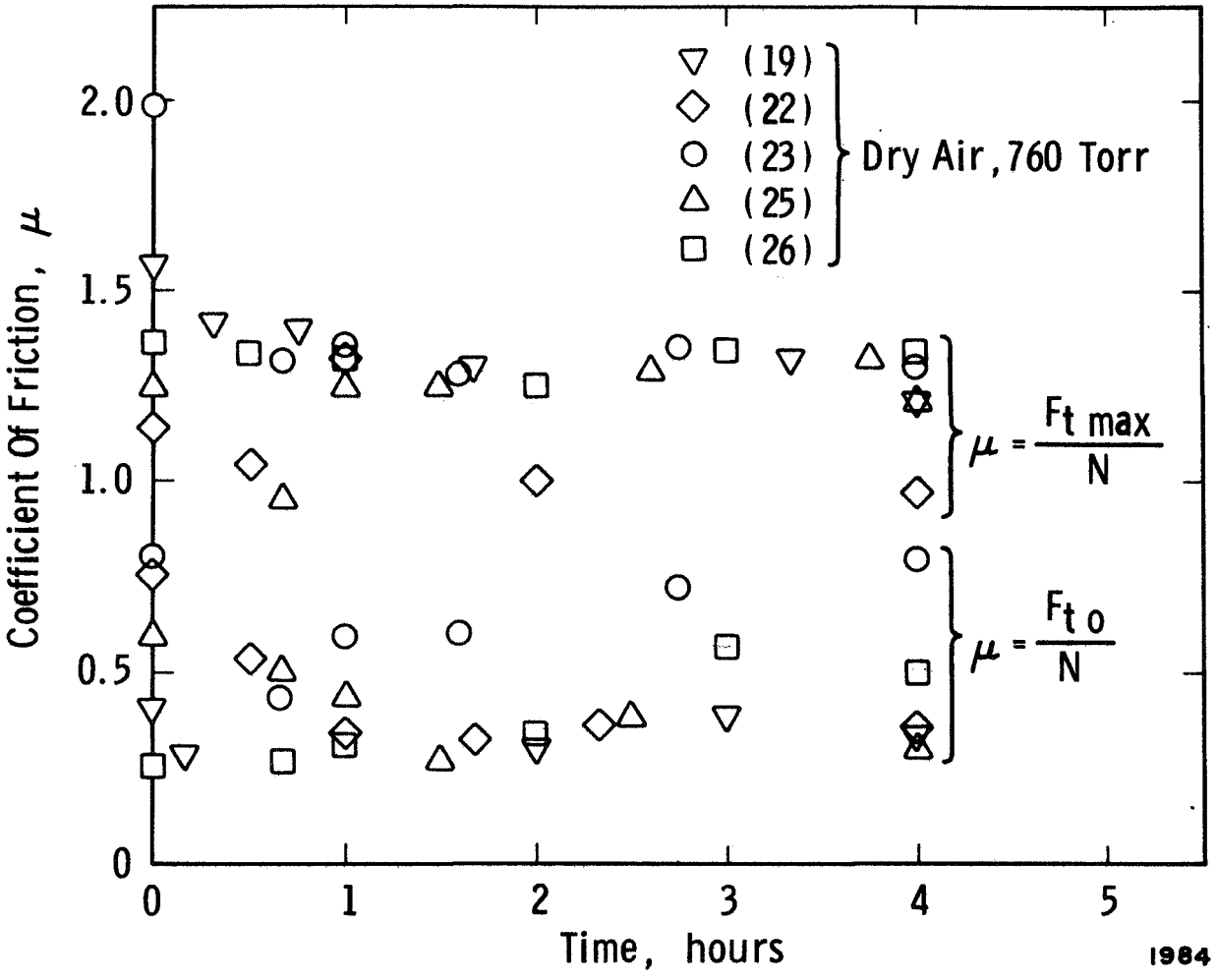

Figure 28. Coefficient Of Friction During Gross Slip Oscillation In Air Based Upon Maximum Tangential Force $F_{t\,max}$ And Upon Force Required To Initiate Slip $F_{t\,o}$